https://doi.org/10.5194/egusphere-2025-6337
Preprint. Discussion started: 3 February 2026

The influence of anthropogenic climate change on Super Typhoon Odette (Typhoon Rai) and its impacts in the Philippines

Ben Clarke[1], Sihan Li[2], Ralf Toumi[3], Nathan Sparks[3]

[1]Centre for Environmental Policy, Imperial College London, UK
[2]School of Geography and Planning, The University of Sheffield, UK
[3]Grantham Institute - Climate Change and the Environment, Imperial College London, UK

Correspondence to: Ben Clarke (b.clarke@imperial.ac.uk)

https://doi.org/10.5194/egusphere-2025-6337
Preprint. Discussion started: 3 February 2026

Abstract. Super Typhoon Odette (Typhoon Rai) made landfall in the Philippines as a category 5 tropical cyclone on 16th December 2021. It brought the compounding effects of extreme rainfall, high winds and storm surge to large parts of the southern-central Philippines, particularly Cebu and Bohol. It was the second costliest typhoon on record for the Philippines up until 2021, causing nearly a billion dollars (US) in direct damage and widespread disruption. In this study, the extreme rainfall and high winds observed during this storm are assessed to determine the influence of anthropogenic climate change (ACC), using three different methods, which focus on the circulation patterns, high rainfall and strong winds associated with Odette, respectively. First, we check that the current generation of higher resolution models used in attribution studies can capture the low sea level pressure anomaly associated with Typhoon Odette and hence can be used to study this type of event. A short analysis then compares such circulation analogues and the associated meteorological extremes over three time periods: past (1950-1970), present (2001-2021), and future (2030-2050), finding evidence of an increase in large-scale precipitation between past and present periods. Second, a multi-method multi-model probabilistic event attribution finds that extreme daily rainfall such as that observed during Typhoon Odette has become about 2 (0.1 to 290) times as likely during the Typhoon season over the southern-central Philippines due to ACC. Third, a large ensemble tropical cyclone hazard model finds that the wind speeds of category 5 landfalling typhoons like Odette have become approximately 70% (3 to 200%) more likely due to ACC. The combined results show that both extreme rainfall and wind speeds in the Philippines due to storms like Odette have become significantly more likely and intense due to ACC, albeit with wide uncertainties on precipitation. Based on these results and compound event attribution theory, we further conclude that ACC has likely more than doubled the likelihood of a compound event like Typhoon Odette and played a key role in amplifying the damages from the event.

https://doi.org/10.5194/egusphere-2025-6337
Preprint. Discussion started: 3 February 2026

1 Introduction

Super Typhoon Odette (henceforth Odette) first formed on Dec 10th 2021 as a tropical depression over the western Pacific. It moved WNW and entered the Philippines' area of responsibility on the 14th, becoming officially named Odette ('Rai' internationally) (ReliefWeb 2024; Santos, 2025). It then rapidly intensified on the 15th and morning of the 16th making multiple landfalls as a category 5 super typhoon throughout the Visayas on the afternoon and evening of the 16th (Chan et al., 2022). It progressed across the Visayas from east to west, bringing heavy rainfall, high winds (Fig. 1), with maximum sustained wind speed of 195 km/h and gusts of up to 270 km/h (Santos, 2025), and storm surges of several metres (Esteban et al., 2023). The transit of the storm resulted in exceptionally disastrous impacts, especially in the provinces of Cebu and Bohol, in which storm surges reached 2.5m and 4m, respectively (Esteban et al., 2023).

The compounding nature of multiple meteorological hazards (heavy precipitation, strong winds, storm surge) from the tropical storm led to flooding, both coastal and rainfall-driven, and the destruction of property, agriculture and infrastructure. 2.1 million homes were damaged, with 425000 considered destroyed entirely (ReliefWeb, 2022). The damages totalled approximately US$915 million, 86000 ha of agricultural land was damaged, and over 300 people were killed (Delforge et al., 2025; Mata et al., 2023), altogether making it the second costliest typhoon to strike the Philippines on record at the time of occurrence after Typhoon Haiyan in 2013. When Typhoon Megi/Agaton struck the Philippines in April 2022, it affected some of the same areas in Leyte province affected by Odette, which compounded impacts further (ReliefWeb, 2022).

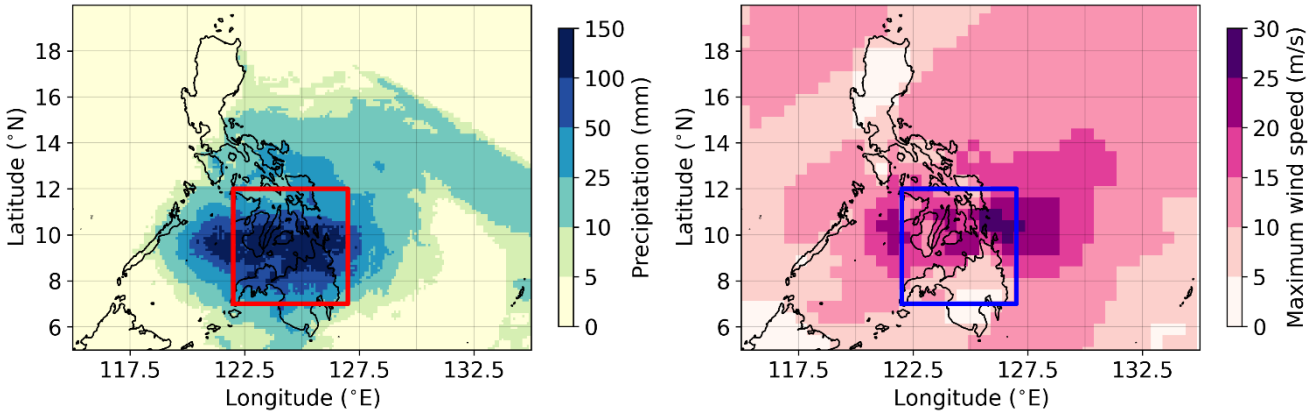

Figure 1: Daily precipitation (mm/day) and maximum wind speeds (m/s) observed on the 16th of December 2021, during the passage of Typhoon Odette over the Philippines. The study region used in Sects.2 & 3 is highlighted in red (left) and blue (right). Precipitation data is from the Multi-Source Weighted-Ensemble Precipitation (MSWEP) and daily maximum wind speeds are from ERA5 (see Sect. 3.2.1). Note: reanalysis datasets struggle to capture the extreme localised winds experienced during category 4 and 5 tropical cyclones, so the values in the right-hand figure are purely illustrative.

https://doi.org/10.5194/egusphere-2025-6337
Preprint. Discussion started: 3 February 2026

The Philippines regularly ranks amongst the nations most affected by climate-related extremes (Eckstein et al., 2021). On average, approximately 19 TCs enter the Philippines 'Area of Responsibility' every year, and 9 TCs make landfall, more than any other nation (Cinco et al., 2016; Santos, 2021). The peak Typhoon season for the Philippines is from June-December, with the fewest experienced around February-March, though they have historically occurred in all months (Cinco et al., 2016), and recently the southern Philippines has seen a dramatic increase in the rate of landfalls from December-February (Basconcillo and Moon, 2021). Research further suggests that there is no significant trend in the rate of landfalling TCs in the Philippines (Cinco et al., 2016), that TCs are moving more slowly (potentially leading to enhanced extreme conditions), and are systematically tracking further north (poleward) (Kossin et al., 2016; Yamaguchi and Maeda, 2020).

Given relatively high exposure and vulnerability to TC hazards, the Philippines is acutely susceptible to influences of anthropogenic climate change upon this. Disentangling the effect of this driver is therefore crucial to enable estimates of the costs of anthropogenic climate change for the Philippines and to assess risks going forwards. Extreme event attribution (EEA) is a field of science that allows the assessment of whether and to what degree anthropogenic climate change influenced the likelihood and/or intensity of an extreme weather event, or some aspects of the event, or a class of similar events at or above a certain rarity/intensity. Several attribution studies exist for TCs around the world, but the number of studies varies significantly by the region in which they occurred. To date, attribution studies for the Western North Pacific (WNP) basin include Typhoons Hagabis (2019), Morakot (2009), Bopha (2012), Mangkhut (2018), Gaemi (2024) and the previously described Typhoon Haiyan (2013), as well as a series of events striking Vietnam in 2020, and the anomalously active cyclone season of 2015 (Fig. 2).

https://doi.org/10.5194/egusphere-2025-6337
Preprint. Discussion started: 3 February 2026

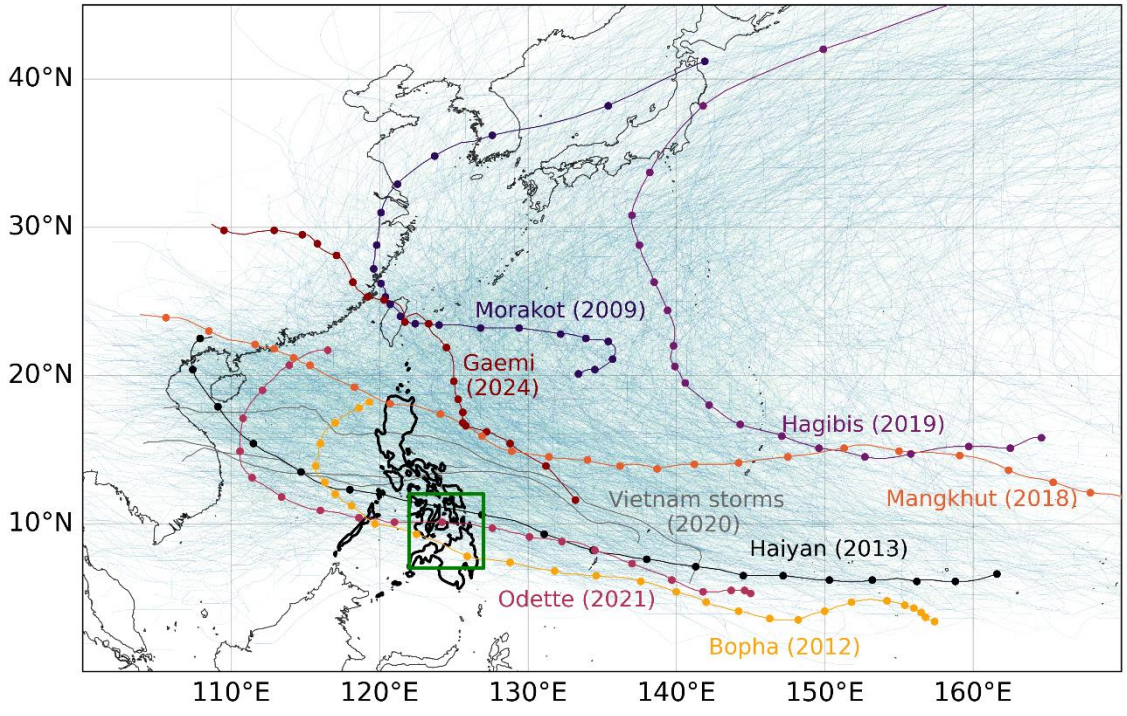

Figure 2: Storm tracks over the observed historical period from IBTrACS (https://www.ncei.noaa.gov/products/international-best-track-archive). The highlighted storm tracks are (to our knowledge) for those with attribution studies, including Odette (studied here), Haiyan, Morakot, Hagibis, Gaemi, and a series of storms striking Vietnam in October 2020. The Philippines is outlined with a ***bold line*** *and the study region for the attribution analysis in Sect. 3 is shown as a green box.*

In this basin, most studies show that anthropogenic climate change has amplified the likelihood and/or intensity of TCs. For instance, in the 2015 TC season, the accumulated cyclone energy was linked to anthropogenically-amplified sea surface temperatures (SSTs) in the eastern and central Pacific (Zhang et al., 2016). The extreme rainfall associated with Typhoon Hagibis, which affected the Tokyo region in 2019, has been tested for an anthropogenic influence using two complimentary methods. A probabilistic approach found that such an event became 67% (15-150%) more likely to occur because of anthropogenic climate change, equating to a fractional attributable risk (FAR) of 0.4 (0.13 – 0.6) and thus approximately US$4 billion in climate change-related damages (Li and Otto, 2022). Meanwhile, a different study using a storyline approach found that anthropogenic climate change amplified the rainfall by around 11% (Kawase et al., 2021). Typhoon Morakot was another major event in the basin, which made landfall in Taiwan in August 2009, bringing extreme rainfall. By simulating the same storm with and without late century (1985-2005) warming, a study found that anthropogenic warming in this period directly led to an increase of approximately 3.5% in Morakot's total rainfall (Wang et al., 2019). In 2020, in central Vietnam, while no

https://doi.org/10.5194/egusphere-2025-6337
Preprint. Discussion started: 3 February 2026

single event caused major impacts, a sequence of typhoon-induced extreme rainfall events led to severe impacts. However, a probabilistic approach found that there was no detectable anthropogenic influence on multi-week rainfall accumulations in central Vietnam (Luu et al., 2021). Finally, a probabilistic analysis of rainfall from Typhoon Gaemi found no significant anthropogenic link in the northern Philippines, but attributable increases in Taiwan and Hunan (Clarke et al., 2024).

In the Philippines, most studies have considered changes in intensity. Typhoons Bopha (2012), Mangkhut (2018) and Haiyan (2013) were studied using a 'pseudo-global warming' approach, which showed that the maximum winds from these storms were increased by 10 m/s, 2 m/s and 2 m/s, respectively, relative to preindustrial times (Delfino et al., 2023). The influence of anthropogenic climate change (ACC) on the intensity and storm surge from Typhoon Haiyan is analysed by multiple other studies (Delfino et al., 2023; Nakamura et al., 2016; Takayabu et al., 2015; Wehner et al., 2019), finding conflicting influences due to the relative contribution of different drivers, as well as storm- and model- dependency. More recent analysis using a synthetic tropical cyclone model, which does not rely on explicit simulation by climate models, found that a typhoon with a landfall maximum wind speed like Haiyan would have been nearly impossible in a world without anthropogenic climate change, with a change in likelihood of such events of a factor of around 45, relative to preindustrial conditions (Sparks and Toumi, 2025). Equivalently, events of such probability have become approximately 3.5 m/s more intense due to ACC at the time of occurrence. Using the same model, a basin-wide analysis of the occurrence of category 4-equivalent storms found that these events now occur 6-7 times per year, compared to 5 times in a preindustrial climate; equivalently, these storms are approximately 4 m/s more intense (Clarke et al., 2024).

In this study, a range of attribution methods are employed to disentangle the influence of anthropogenic climate change on the compounding hazards of Odette. First, in Sect. 2 the use of circulation analogues is explored. This method employs the observed circulation patterns during Odette and studies comparable events, i.e. those with similar sea level pressure anomaly patterns, in high resolution global climate models, under climate conditions of past, present and future. This method serves two purposes, assessing: a) whether the current generation of high resolution climate models (with resolution on par of those analysed in the method of Sect. 3), can capture the circulation patterns leading to events comparable to Odette; and b) whether there are changes in the extreme meteorological conditions associated with such circulation patterns under different levels of anthropogenic forcing. Second, in Sect. 3, a probabilistic event attribution for extreme rainfall as observed during Odette is conducted. This comprises a statistical analysis of changing rainfall extremes using the observed magnitude of Odette as a basis. It employs both gridded observational products and regional climate models to assess how rainfall extremes are changing due to changes in global mean surface temperature (GMST). Third, in Sect. 4, the changing likelihood of landfalling category 5 TCs is modelled using a synthetic tropical cyclone model, based on IBTrACS observations. This is the Imperial College Storm Model – IRIS – described in Sparks and Toumi (2024), a Haiyan attribution study (Sparks and Toumi, 2025) and further in Sect. 4.

https://doi.org/10.5194/egusphere-2025-6337
Preprint. Discussion started: 3 February 2026

Taken together, this study combines several complementary approaches to attributing the meteorological hazards associated with Odette: a conditional attribution focusing on events of similar circulation patterns, a probabilistic analysis of changing likelihoods of precipitation extremes, and a probabilistic analysis grounded in historical events and physical understanding of strong wind extremes. Finally, the implications of this work for the attribution of impacts from Odette are discussed.

2 Circulation analogues

Circulation (or 'flow') analogues are other occurrences of similar atmospheric conditions, often based on atmospheric pressure levels, to that in which the event in question occurred (Faranda et al., 2022; Ginesta et al., 2023; Harrington et al., 2019; Vautard et al., 2016; Yiou et al., 2017). Comparing the meteorological conditions under similar circulation regimes but at different times (or warming levels) helps to control for any changes in such dynamics. This enables us to disentangle only the direct 'thermodynamic' contribution of warming to an event, which is generally larger in magnitude and less subject to deep uncertainties around changes in complex atmospheric processes (Shepherd, 2016). Here, testing for the existence of circulation analogues within models also helps to evaluate whether models can capture such conditions, and gives one assessment of changing extremes from events like Odette.

2.1 Data and methods

We use observation-based reanalysis ERA5 (Hersbach et al., 2020) to characterise the anomalously low sea level pressure patterns associated with Odette (Fig. 3). We then use the same set of variables from climate model simulations models to investigate the possible changes of events similar to Odette. These simulations are the High-Resolution Model Intercomparison Project (HighResMIP) SST-forced model ensemble (Haarsma et al., 2016), from the sixth phase of the Coupled Model Intercomparison Project (CMIP6) generation experiments, with simulations spanning from 1950 to 2050 (Table 1). HighResMIP provides multi-model and multi-resolution simulations (Haarsma et al., 2016). Under the CMIP6 HighResMIP protocol, the European Union Horizon 2020 project, PRIMAVERA (PRocess-based climate sIMulation: AdVances in high resolution modelling and European climate Risk Assessment), has provided global atmospheric general circulation model (AGCM) simulations at CMIP6-standard resolution (~100 km) and higher resolutions (~25 km). These simulations enable scientists to analyse TCs and assess the reliability of changes in TC rainfall across a variety of numerical models and spatial scales (Roberts et al. 2020). The SST and sea ice forcings for the period 1950-2014 are obtained from the 0.25° x 0.25° Hadley Centre Global Sea Ice and Sea Surface Temperature dataset that are area-weighted regridded to match the climate model resolution (Table 1). For the 'future' time period (2015-2050), SST/sea-ice data are derived from RCP8.5 (CMIP5) data and combined with greenhouse gas forcings from SSP5-8.5 (CMIP6) simulations (see Sect. 3.3 of Haarsma et al. 2016 for further details).

https://doi.org/10.5194/egusphere-2025-6337
Preprint. Discussion started: 3 February 2026

Model	Resolution	Institute
CMCC-CM2-VHR4	~25 km	Fondazione Centro Euro-Mediterraneo sui Cambiamenti Climatici
CMCC-CM2-HR4	~100 km	Fondazione Centro Euro-Mediterraneo sui Cambiamenti Climatici
CNRM-CM6-1-HR	~50 km	Centre National de Recherches Meteorologiques
CNRM-CM6-1	~100 km	CNRM-CERFACS
EC-Earth3P-HR	~40 km	EC-Earth-Consortium
EC-Earth3P	~80 km	EC-Earth-Consortium
HadGEM3-GC31-HM	~25 km	UK Met Office, Hadley Centre
HadGEM3-GC31-MM	~60 km	UK Met Office, Hadley Centre
HadGEM3-GC31-LM	~135km	UK Met Office, Hadley Centre
MPI-ESM1-2-XR	~60 km	Max Planck Institute for Meteorology
MPI-ESM1-2-HR	~100 km	Max Planck Institute for Meteorology

Table 1: List of HighResMIP models used in the study, the spatial resolution of each, and the institute in which the model was developed.

To assess the properties of comparable events at different warming levels, we search for similar circulation patterns in different time periods. We consider a "past" 20-year time slice of 1950-1970, a "present" 20-year time slice of 2001–2021, and a "future" 20-year time slice of 2030-2050. The past represents a world with a weaker anthropogenic influence on climate than the present, the present refers to the current climate conditions, and the future represents a future world with further warming and enhanced anthropogenic climate change compared to the present. We note that, due to the limited availability of long-term

https://doi.org/10.5194/egusphere-2025-6337
Preprint. Discussion started: 3 February 2026

datasets from HighResMIP models required for analogue analysis, these periods represent a smaller change in GMST than in sections 3 and 4, which extrapolate observed trends over the full warming range of approximately 1.2°C between the present and preindustrial period.

The circulation pattern used to search for analogues is defined as the spatial pattern of sea level pressure (SLP) anomaly, with respect to climatological period 1981-2010, over the domain of interest (5-20 °N, 115-130 °E) on December 16th 2021 (Fig. 3a, dashed black box). For consistency with section 3, the analogue search was conducted over the wider TC season of June-December. Analogues are assessed using the spatial correlation between all daily SLP patterns from the models and the event circulation pattern, defined above, with a gap of at least 5 days between selected events to ensure independence. Finally, the meteorological conditions (rainfall accumulations, mean and maximum wind speeds), are averaged over the region most affected by Typhoon Odette (7-12 °N, 122-127 °E, Fig. 3a – blue dashed box), consistent with the analysis in section 3.

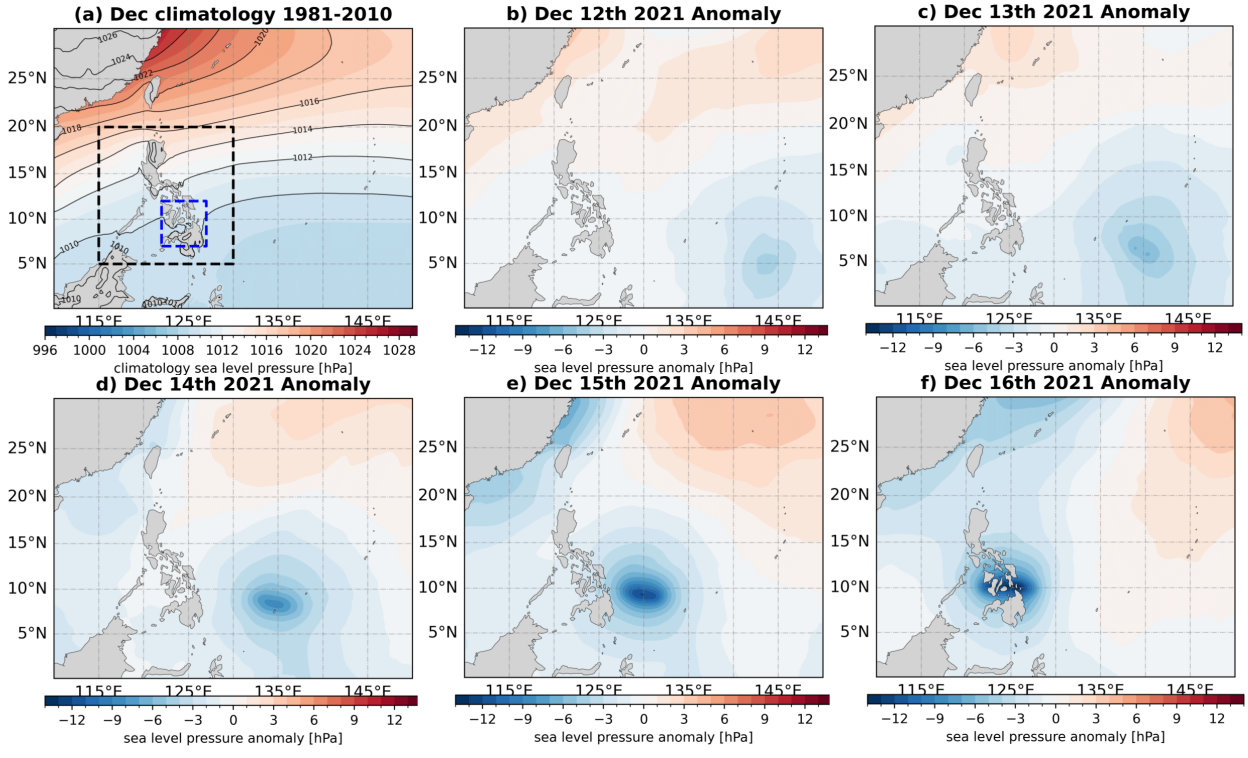

Figure 3: Sea level pressure (SLP) fields over the Philippines from ERA5 reanalysis (in hPa). a) The climatological mean over 1981-2010 December. The black dashed box highlights the region used to search for circulation analogues and the blue dashed box shows the region used to assess meteorological extremes, consistent with section 3. (b-e) The evolution of anomalous sea level pressure (w.r.t. climatological mean shown in panel a) associated with Typhoon Odette from December 12-16th 2021.

https://doi.org/10.5194/egusphere-2025-6337
Preprint. Discussion started: 3 February 2026

2.2 Results

Figure 3 shows sea level pressure (SLP) evolution associated with Odette. The early development of Odette (panel b) is visible as a localised area of negative sea-level pressure anomalies (~-4 hPa) southeast of the Philippines on the 12th of Dec. The negative anomalies intensified (~-6 hPa) on the 13th, and the system became more organized. By the 14th, the low-pressure anomaly had deepened significantly (~-8 to -10 hPa), with a well-defined structure, and by the 15th, the system reached its peak intensity with central pressure anomalies exceeding -12 hPa. This extreme anomaly signifies the fully developed typhoon with tightly packed isobars, consistent with the associated heavy rainfall and strong winds. On the 16th, Odette made landfall in the Philippines, and the typhoon's core pressure remained anomalously low (~-10 to -12 hPa), The persistence of strong negative anomalies over the region reflects the typhoon's ongoing impact.

2.2.1 Model fidelity

Figure 4 displays the SLP anomaly patterns from the HighResMIP models, each showing the pattern on the day with the highest spatial correlation to the observed anomalies during Typhoon Odette's landfall on December 16th, 2021. The panels illustrate how different models simulate the SLP anomalies in the region (5°–20°N, 115°–130°E), providing insight into the models' ability to capture the cyclone's intensity and structure (anomalies for a wider region up to 135°E are shown in Fig. A1, giving similar results). The observed SLP anomalies highlight a strong negative anomaly (~-12 hPa) centred over the Philippines, marking the typhoon's core. CMCC-CM2-HR4 and CMCC-CM2-VHR4 capture a negative anomaly over the Philippines, but the intensity and spatial extent are less pronounced compared to observations. The higher-resolution version CNRM-CM6-1-HR better represents the observed central low, while the lower-resolution version CNRM-CM6-1 shows a weaker anomaly. Both EC-Earth3P and EC-Earth3P-HR show negative anomalies, but the higher-resolution version of the model (HR) offers a more concentrated anomaly, aligning more closely with the observed typhoon core. The MPI models simulate a similar anomaly pattern but much weaker compared to the observed. Among all models, the high-resolution HadGEM3-GC31-HM best reproduces the observed anomaly intensity and spatial pattern, closely matching the central low (~-12 hPa). Higher-resolution models generally provide more accurate simulations of the SLP anomalies, capturing the intensity and compact structure of Typhoon Odette; whereas models with coarser resolutions tend to underestimate the strength of the negative anomaly and spread it over a larger area. These results further demonstrate the importance of high-resolution modelling in accurately representing extreme tropical cyclone events and their anomalously low sea level pressure patterns. Given these results, the following analysis only uses the high-resolution versions (i.e. CMCC-CM2-VHR4, CNRM-CM6-1-HR, EC-Earth3P-HR, and HadGEM3-GC31-HM), all of which have <=50km horizontal resolution, as detailed in Table 1, while excluding the MPI models given the weak comparison with the observed.

https://doi.org/10.5194/egusphere-2025-6337
Preprint. Discussion started: 3 February 2026

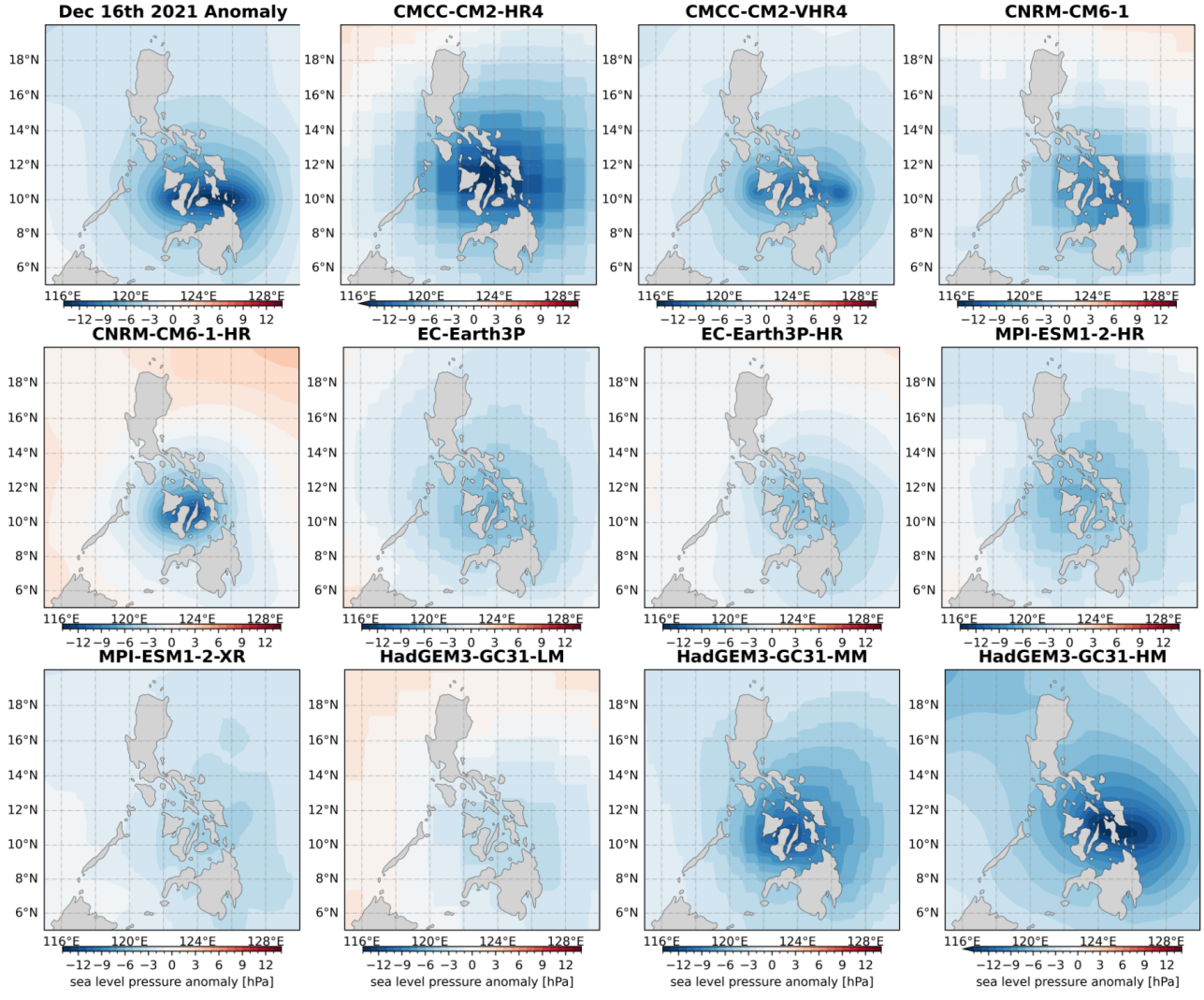

Figure 4: For each model, the sea level pressure anomaly patterns over (5-20 °N, 115-130 °E) with the highest spatial correlation to Dec 16th 2021 during Odette landfall is shown.

Figure A2 presents the composite maps of the top 5 ranking analogous for each of the selected models across the past, present and future. Across different periods, the models generally maintain a consistent pattern, suggesting a robust ability to simulate this kind of pattern across different time slices. However, the 2030-2050 projections sometimes show a shift in the anomaly's strength and location, suggesting possible future changes in cyclone behaviour. For example, CMCC-CM2-VHR4 predicts slightly stronger and more expansive anomalies, which could indicate more intense and larger spatial extent of cyclones, whereas CNRM-CM6-1-HR predicts a more expansive but weaker anomaly. Both EC-Earth3P-HR and HadGEM-GC31-HM

https://doi.org/10.5194/egusphere-2025-6337
Preprint. Discussion started: 3 February 2026

predicts a less expansive and slightly weaker anomaly. The differences among models highlight the uncertainty in projections and the importance of using multiple models to capture the range of possible future outcomes.

Despite the overall consistency in capturing the anomaly, the variability between models and across time periods indicates uncertainty in both the models' ability to simulate this kind of event and in future projections. The range of different model behaviours illustrates the challenges in predicting the exact impact of anthropogenic climate change on tropical cyclone behaviour in this region with this set of models. In summary, the comparison of the observed SLP anomaly with the model ensemble suggests that this set of climate models can simulate the general circulation features of such extreme cyclonic events, though with some variation in intensity and location. These results further highlight the importance of using a multi-model ensemble to capture the range of potential future outcomes, as has been done in this study.

2.2.2 Hazard results

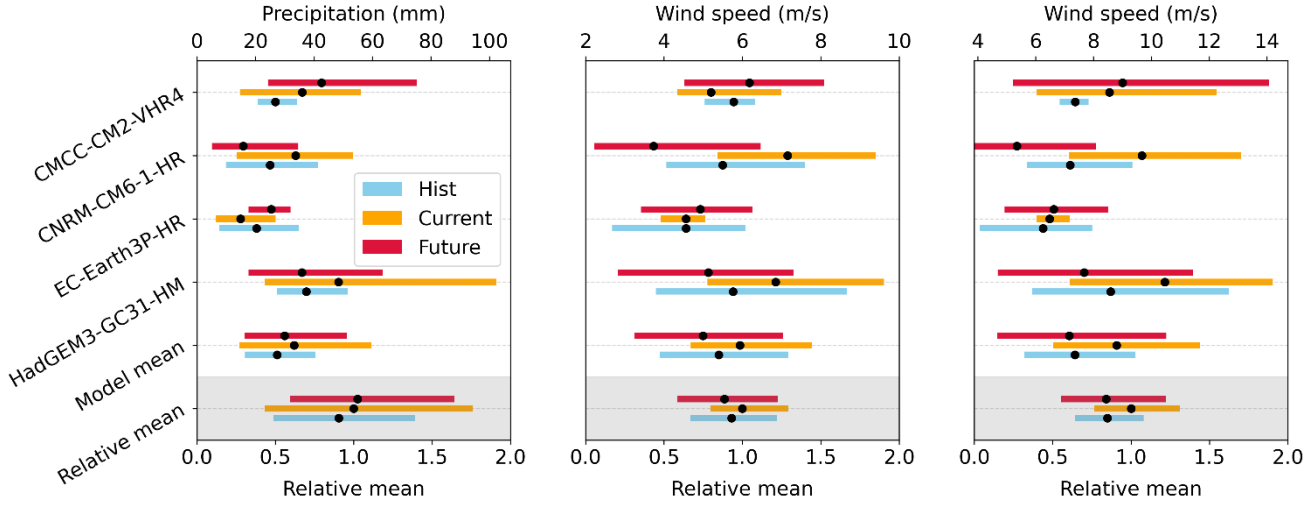

Figure 5: Daily precipitation (left), daily mean wind speed (middle), and daily maximum wind speed (right), averaged over 7-12 °N, 122-127 °E (same as Section 3) corresponding to the top 5 ranking analogues shown in Fig. A2, for past (black), present (red) and future (blue). For each model, the dot represents the mean of the 5 values and the spread represents the minimum and maximum. For the 'model mean' results, the dot and spread represent the unweighted mean of all model's respective mean, minimum and maximum values. For the 'relative mean' results, the dot and spread represent the unweighted mean of mean, minimum and maximum values after normalising all values with respect to the current day mean (such that the 'current' mean value for each model is 1).

Given the circulation analogues shown in Fig. A2, Fig. 5 presents the corresponding shift of daily precipitation, daily maximum wind speed, and daily mean wind speed for the selected models across the three different time periods. There is a general

https://doi.org/10.5194/egusphere-2025-6337
Preprint. Discussion started: 3 February 2026

increase in daily precipitation from 1950-1970 to 2001-2021 across most models, with only one model (EC-Earth3P-HR) showing a slight decrease between these periods. To compare and quantify this effect across models, we first assess the relative values in all periods for each model by dividing all values by the 'current' period mean. This returns all "current" mean values as 1 and the past and future values (along with all minima and maxima) are each some fraction of the present-day mean value. These values are then averaged to give a mean relative change between the periods (Fig. 5), giving past values of 0.906 (0.488 to 1.392) for the past, 1 (0.432 to 1.762) for the present, and 1.024 (0.593 to 1.644) for the future. This suggests an increase of approximately 10% in precipitation between past and current conditions. This suggests a trend toward wetter extremes given similar circulation conditions, consistent with thermodynamic understanding from Clausius–Clapeyron. Comparing 2001-2021 to 2030-2050, the picture is less clear. Two models (CMCC-CM2-VHR4 and EC-Earth3P-HR) predict a slight increase, while the other two (CNRM-CM6-1-HR and HadGEM3-GC31-HM) predict a slight decrease. When combined, there is an overall relative increase between the past and future periods of approximately 13%, and ~2% between present and future.

For both daily mean and maximum wind speeds, the analogues give regionally averaged values far below (approximately an order of magnitude) those expected of high category TCs (Fig. 5). This may be due to the inability of climate models of the resolutions used to simulate such extremes, with key dynamical processes such as deep convection occurring at subgrid scales. Another related factor may be in the application of the circulation analogue method. In accordance with Sect. 3, a relatively small region is used to assess the meteorological extremes, which may mean that events similar to Odette in SLP pattern but spatially displaced in the resultant extremes are not fully captured. This would also affect the most intense precipitation around the storm centre but have less influence on the larger scale rainfall that is assessed here, which should at least be partially captured in the assessed region. Consequently, while the changes in winds broadly follow similar those in rainfall, we do not draw any conclusions from model results here primarily due to the inability of models to simulate these extremes.

This section has two main conclusions. First, the existence of analogues in the current generation of climate models indicates that they are applicable for studying certain elements of TCs but remain inapplicable for others. For instance, the phenomena known to generate the most extreme winds and localised rainfall from TCs occur at scales of ~1-10 km, which requires higher resolution modelling (at convection-permitting scale) to resolve. The damage from winds also tends to result from the most intense localised magnitudes, making the HighResMIP models unsuitable for analysing extreme winds. However, rainfall over a larger region, over tens to hundreds of kilometres, which the HighResMIP models can resolve, is still relevant to many of the impacts of such events. Specifically, in the following section climate models with similar or higher resolution to those studied here are used to analyse changes in extreme rainfall. This section therefore provides additional confidence that the probabilistic event attribution modelling conducted in this paper is relevant for this study of the influence of anthropogenic climate change on Typhoon Odette. Second, analogues give preliminary evidence that anthropogenic climate change has led to an increase in precipitation of approximately 10% under similar circulation conditions over the past few decades.

https://doi.org/10.5194/egusphere-2025-6337
Preprint. Discussion started: 3 February 2026

3. Attribution of extreme rainfall using probabilistic event attribution

3.1 Data and methods

3.1.1 Event definition

To statistically model how events like Odette have changed as the world has warmed, an extreme index is used to define historical events. This is based on spatiotemporal aspects of the observed event. Odette brought extreme rainfall to the Visayas in the southern-central Philippines (Figs. 1&2). While the impacts were only experienced on land, the land masses in this region are extremely complex on small scales, and most gridded observational products and regional climate models are too coarse to capture these coastal terrain features accurately. As a result, we defined a region bounded by 7 - 12°N, 122 - 127 °E, including both land and ocean areas. We use single day rainfall maxima in accordance with observations of the extreme rainfall, which occurred primarily on Dec 16th, 2021 (Fig. 1). Finally, we consider such maxima over two time-windows of the year: December only, and June-December. The former enables an assessment of changes in TCs at the end of the season when such extreme TCs are less common but are seeing a marked increase in frequency. The latter period captures the active TC season for most of the Philippines, ensuring that the most occurrences of high precipitation are associated with TCs. Using multiple timescales further aids by testing the sensitivity of results to the event definition selection. While this index will include non-TC events, it is worthy of note that, across the four observational datasets used (Sect. 3.1.2), TC events account for 70-80% of all extreme rainfall events in the studied period. We therefore have high confidence that any detected changes in extreme precipitation are mostly due to changes in TCs.

3.1.2 Data

We use a range of gridded observational and reanalysis products: the ERA5 reanalysis (Hersbach et al., 2020), from which we use daily precipitation and maximum wind speed data; the Multi-Source Weighted-Ensemble Precipitation (MSWEP) v2.8 dataset (updated from Beck et al., 2019) at 0.1° spatial resolution, available from 1979 to ~3 hours from real-time; the "Climate Hazards Group InfraRed Precipitation with Station data" (CHIRPS; Funk et al., 2015), at 0.05° resolution, from 1981 to 31st Jan 2024; the Global Precipitation Climatology Centre (GPCC) Full Data Daily Product Version 2022 of daily global land-surface precipitation totals at 1.0° (Markus et al., 2022); finally, as a measure of anthropogenic climate change we use the (low-pass filtered) global mean surface temperature (GMST) from the Goddard Institute for Space Science (GISS) surface temperature analysis (GISTEMP; Hansen et al., 2010 and Lenssen et al., 2019).

We also use 2 multi-model ensembles from regional climate modelling experiments with model domains covering the Philippines. These simulations are composed of historical simulations up to 2005 and extended to the year 2100 using the RCP8.5 scenario under CMIP5 forcings, and include: the Coordinated Regional Climate Downscaling Experiment-Southeast

https://doi.org/10.5194/egusphere-2025-6337
Preprint. Discussion started: 3 February 2026

Asia (CORDEX-SEA) (0.22° resolution, SEA-22) multi-model ensemble (Tangang et al., 2020), consisting of 8 simulations resulting from pairings of 4 Global Climate Models (GCMs) and 3 Regional Climate Models (RCMs); and the Coordinated Regional Climate Downscaling Experiment-East Asia (CORDEX-EAS) (0.22° resolution, EAS-22) multi-model ensemble (Kim et al., 2021), consisting of 6 simulations resulting from pairings of 3 Global Climate Models (GCMs) and 2 Regional Climate Models (RCMs).

These climate models are evaluated against the observations in their ability to capture:

1. Seasonal cycles: Qualitative comparison of seasonal cycles based on model outputs against observations-based cycles, discarding models that exhibit multi-modality and/or ill-defined peaks in their seasonal cycles.

2. Spatial patterns: Similarly, models that do not match the observations in terms of the large-scale annual mean precipitation patterns are excluded, with a focus on the E-W gradient of rainfall across the Philippines.

3. Parameters of the fitted statistical models (See Sect. 3.1.3): Models are discarded if the model and observation parameters ranges do not overlap.

The models are labelled as ‘good’, ‘reasonable’, or ’bad’ based on their performances in terms of the three criteria discussed above, and models labelled ‘bad’ in any of the three criteria are discarded. In total, 8 and 6 simulations were evaluated from CORDEX-SEA and CORDEX-EA, respectively. For December event definition, 5/8 SEA models and 4/6 EA models passed the evaluation. For June-December, 4/8 and 4/6 from each ensemble, respectively, passed (see Tables B1 and B2, Figs. B2-B5).

3.1.3 Statistical methods

To estimate the influence of GMST, we statistically model the event under study using a nonstationary generalised extreme value (GEV) distribution with GMST as covariate. For extreme rainfall, the GEV distribution is assumed to scale exponentially with the covariate, with the dispersion (the ratio between the standard deviation and the mean) remaining constant over time. This formulation reflects the form of the Clausius Clapeyron relation, which implies that precipitation scales exponentially with temperature (O’Gorman and Schneider, 2009; Trenberth et al., 2003). The parameters of the statistical model are estimated using maximum likelihood. For each time series, including all observational datasets and climate models, we use the fitted nonstationary model to calculate the return period and intensity of the event under study for the 2021 GMST and for 1.2 °C cooler GMST: this allows us to compare the climate of at the time of occurrence and of the preindustrial past (defined as 1850-1900), by calculating the probability ratio (PR; the factor-change in the event's probability) and change in intensity of the event.

https://doi.org/10.5194/egusphere-2025-6337
Preprint. Discussion started: 3 February 2026

Results from observations and models that pass the evaluation tests are then synthesised into a single attribution statement, including a probability ratio and a change in intensity. This involves three steps. First, a representation error is added in quadrature to the observations, to account for the difference between observations-based datasets that cannot be explained by natural variability, and the results from the observational-based products are averaged (throughout, probability ratios are averaged using the logarithmic mean). Next, a term to account for inter-model spread is added in quadrature to the natural variability of the models, which are also averaged. This consists of a weighted mean using the (uncorrelated) uncertainties due to natural variability plus the term representing inter-model spread. Where no finite estimate of the upper bound of an infinite is obtained, a finite upper bound is inferred by using the distance between the best estimate and lower bound to estimate the standard deviation of the distribution, and so to estimate the width of a six-sigma interval above the best estimate (Otto et al., 2024). This procedure is performed in reverse where the lower bound is initially estimated as 0. Where the lower and upper bounds equal 0 and infinity, respectively, no useful information is obtained, and the dataset is discarded from the synthesis. In this study, one SEA model, NorESM1-M RegCM4-7, was removed from the December synthesis for this reason. Third, observation-based products and models are combined into a single result in two ways. Firstly, common model uncertainties beyond the inter-model spread that is depicted by the model average are neglected, and we compute the weighted average of models and observations. As, due to common model uncertainties, model uncertainty can be larger than the inter-model spread, we also estimate the more conservative estimate of an unweighted, direct average of observations and models. For additional details, all methods for observational and model analysis and for model evaluation and synthesis follow the protocol described in Philip et al. (2020), with supporting details found in van Oldenborgh et al. (2021) and Ciavarella et al. (2021).

3.2 Results

3.2.1 Observational analysis

December

Table 2 (and Fig. B1) show the trends in December maxima of 1-day rainfall over the study region for four gridded observational and reanalysis datasets. All datasets show a strong increase in the likelihood of events with 1-day rainfall at least as extreme as Odette with global warming, with estimates of the PR ranging from 3.8 (0.1 to 470) in ERA5 to over 1000 in CHIRPS and MSWEP, (the latter of which is statistically significant at the 95% confidence level). These are consistent with strong increases over time visible in the loess smoothed trends for all datasets, except for ERA5 prior to ~1960 (Fig. B1). Overall, based on an approximate mean of all estimates, a return period of 20 years is used to characterise the event in model analysis.

Dataset	Observed event	Trend due to GMST

https://doi.org/10.5194/egusphere-2025-6337
Preprint. Discussion started: 3 February 2026

	Magnitude (mm)	Return period (95% C.I.)	Probability Ratio (95% C.I.)	Change in magnitude (%) (95% C.I.)
ERA5	83.26	30.61 (9.9 – 12625)	3.8 (0.037 to 104)	31.3 (-22.6 to +135)
CHIRPS	76.48	11.64 (4.5 – 206.82)	1594 (0.59 to inf)	64.5 (-10.5 to +157)
MSWEP	78.94	20.06 (5.55 – 757.37)	**1840 (1.28 to inf)**	**98.4 (+4.08 to +321)**
GPCC	76.98	19.58 (5.76 – 522.38)	9.65 (0.41 to inf)	43.9 (-14.3 to +160)

Table 2: Observed event magnitude and estimated return period of the events in the present climate (2021), the estimated probability ratio for an event of equivalent magnitude, and the change in magnitude of an event of equivalent return period due to global warming of 1.2 °C, across four datasets. 95% confidence intervals are shown in brackets. Increasing (decreasing) trends with increasing GMST are highlighted in blue (orange). ***Bold*** *text and darker shading indicate where the estimate is statistically significant at the 95% confidence level.*

June-December

Figure 6 and Table 3 show the trends in June-December maxima of 1-day rainfall over the study region for four gridded observational and reanalysis datasets. Datasets show mixed trends in the likelihood of events at least as extreme as Odette with global warming. Estimates of the probability ratio range from a decrease of a factor of 2 (0.04 to 270) in MSWEP up to an increase of infinity (0.05 to inf) in CHIRPS, the latter suggesting the event would have been statistically virtually impossible without global warming. Differences between the datasets are evident from the loess smoothed trends in Fig. 6, in which CHIRPS and ERA5 show generally monotonic increasing trends since around 1980, while MSWEP and GPCC show variable trends. This is further reflected in the return period curves in Fig. 6, in which CHIRPS and ERA5 show a strong correspondence between the data and fitted model, whereas the most extreme events are represented poorly by the statistical model in MSWEP and GPCC. Overall, none of the estimated changes are statistically significant at the 95% confidence level and, combining all estimates, again a return period of 20 years is used to characterise the event in model analysis.

Dataset	Observed event	Trend due to GMST

https://doi.org/10.5194/egusphere-2025-6337
Preprint. Discussion started: 3 February 2026

	Magnitude (mm)	Return period (95% C.I.)	Probability Ratio (95% C.I.)	Change in magnitude (%) (95% C.I.)
ERA5	83.26	24.3 (9.9 – 135.0)	1.56 (0.32 to 20.0)	8.38 (-19.3 to +45.8)
CHIRPS	76.48	31.4 (6.7 – inf)	inf (0.0001 to inf)	23.0 (-30.2 to +72.1)
MSWEP	78.94	21.1 (7.4 – 174.6)	0.47 (0.03 to 239.5)	-13.3 (-46.8 to +53.4)
GPCC	76.98	13.8 (4.0 – 74.4)	0.6 (0.07 to 10^9)	-8.80 (-49.1 to +55.6)

Table 3: Observed event magnitude and estimated return period of the events in the present climate (2021), the estimated probability ratio for an event of equivalent magnitude, and the change in magnitude of an event of equivalent return period due to global warming of 1.2 °C, across four datasets. 95% confidence intervals are shown in brackets. Increasing (decreasing) trends with increasing GMST are highlighted in blue (orange).

https://doi.org/10.5194/egusphere-2025-6337
Preprint. Discussion started: 3 February 2026

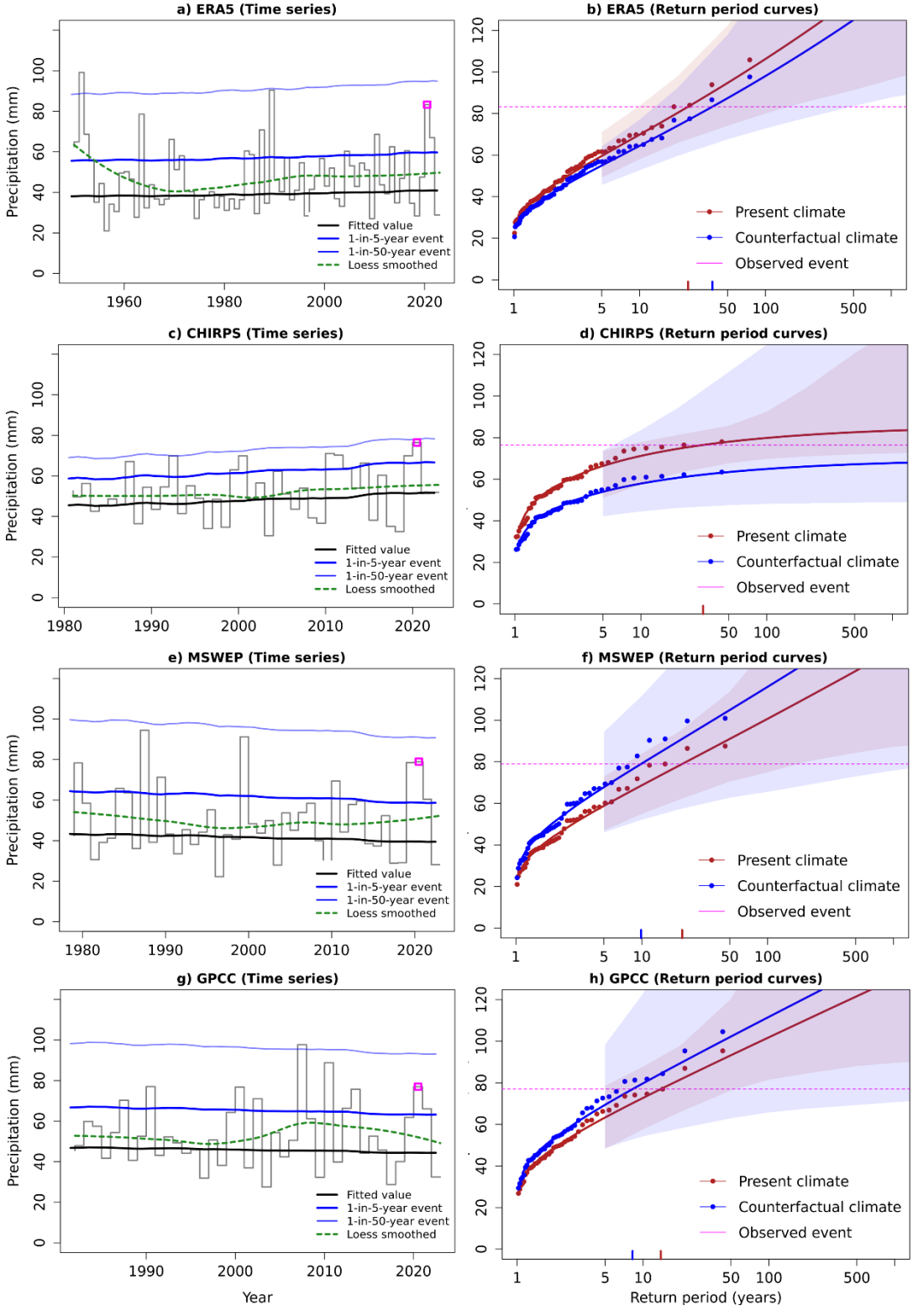

https://doi.org/10.5194/egusphere-2025-6337
Preprint. Discussion started: 3 February 2026

Figure 6: Times series and statistical fits in the four observational datasets, ERA5, CHIRPS, MSWEP and GPCC for June-December. a) Shows the time series (grey) and fitted statistical model trend (black), with the event associated with Odette highlighted in purple. The modelled 5- and 50-year events are shown as dark and light blue lines, respectively, and the loess smoothed trend is shown by the green dashed line. b) Shows the GEV fit to the ERA5 data at two levels of the covariate GMST: in 2021 (red curve) and in a 1.2 °C cooler climate (blue curve). The dashed purple line shows the magnitude of Odette. The small blue and red lines on the x axis show the estimated return period of the event in the preindustrial and present climates, respectively. c) and d), e) and f), g) and h): As in (a) and (b) for CHIRPS, MSWEP and GPCC data.

From observations alone, there is a consistent trend showing that global warming has increased the likelihood and intensity of extreme rainfall events like Typhoon Odette in December alone. However, it remains unclear whether this effect extends to the wider TC season of June-December due to disagreement between datasets. Furthermore, such analysis of observations alone constitutes a trend detection rather than an attribution, as it represents only a single realisation of the changing climate. Therefore, to elucidate the attributable link between anthropogenic climate change and events like Typhoon Odette, the results from observations for each event definition are synthesised with the respective results from climate models. This gives an overall estimate of the influence of anthropogenic climate change that is not as heavily dependent on individual data sources.

3.2.2 Synthesis and conclusions

The influence of anthropogenic climate change on the rainfall from Odette is estimated, for each event definition, by calculating the probability ratio (for an event of equivalent intensity) and the change in intensity (for an event of equivalent likelihood) using a combination of gridded observation-based datasets and climate models. For climate models, changes are assessed for the 1-in-20-year events for both event definitions, based on those estimated from observations in section 3.2.1. Using the return period to select the event magnitude for each model is equivalent to a single-quantile bias correction. The same statistical modelling procedure is used for each individual dataset, as laid out in section 3.1.3. Figs. 7 & 8 show the resultant changes in probability and intensity for the observations and models. The synthesis result displayed is computed from the weighted average of models and observations, and the white bar around the magenta bar indicates the unweighted average of uncertainty bounds of the model and observational estimates.

https://doi.org/10.5194/egusphere-2025-6337
Preprint. Discussion started: 3 February 2026

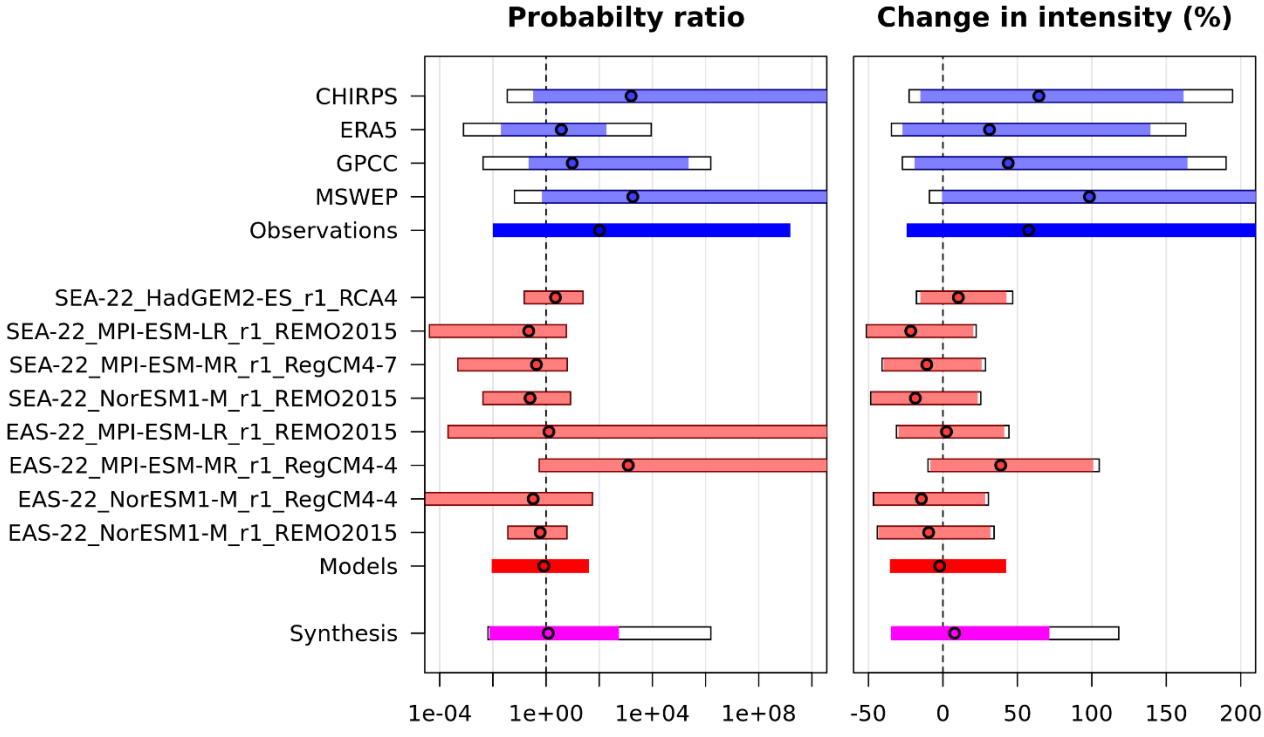

Figure 7: Synthesis of (a) probability ratios and (b) intensity changes for observations (blue) and models (red) when comparing the 1-day maximum December precipitation that occurred in 2021 with a 1.2 °C cooler climate. The dark blue bar shows the synthesised results of the observation-based products. The dark red bar shows the model synthesis, consisting of a weighted mean using the (uncorrelated) uncertainties due to natural variability. The magenta bar shows the full synthesis. The white bar around the magenta bar indicates the unweighted average of uncertainty bounds of the model and observational estimates.

https://doi.org/10.5194/egusphere-2025-6337
Preprint. Discussion started: 3 February 2026

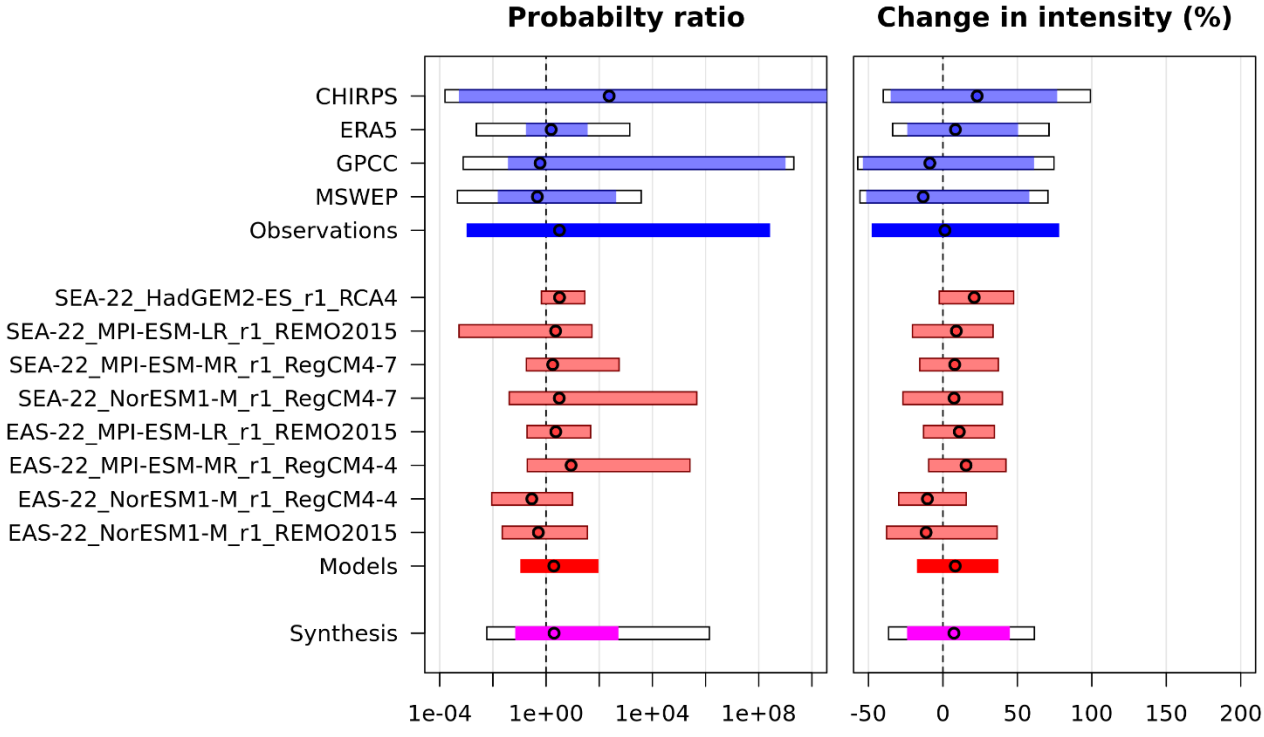

Figure 8: Synthesis of (a) probability ratios and (b) intensity changes for observations (blue) and models (red) when comparing the 1-day maximum June-December precipitation that occurred in 2021 with a 1.2 °C cooler climate. The dark blue bar shows the synthesised results of the observation-based products. The dark red bar shows the model synthesis, consisting of a weighted mean using the (uncorrelated) uncertainties due to natural variability. The magenta bar shows the full synthesis. The white bar around the magenta bar indicates the unweighted average of uncertainty bounds of the model and observational estimates.

https://doi.org/10.5194/egusphere-2025-6337
Preprint. Discussion started: 3 February 2026

Time period (data type)		**Probability ratio** (95% confidence intervals)	**Intensity change (%)** (95% confidence intervals)
Past-Present	Observations	101.6 (0.018 to 10^9)	57.5 (-19.7 to +214)
	Models	0.83 (0.016 to 22.8)	-2.17 (-31.0 to +37.8)
	Synthesis (weighted)	1.22 (0.014 to 301)	7.85 (-30.2 to +66.8)
	Synthesis (unweighted)	11.1 (0.011 to 10^6)	27.7 (-27.4 to +114)
Present-Future	**Models only**	1.03 (0.37 to 2.13)	0.39 (-10.4 to +9.87)

Table 4: Summary of synthesised results for events like Typhoon Odette in the December period, due to warming of 1.2 °C, corresponding with the synthesis bars shown in Fig. 7. Increases (decreases) in likelihood and intensity due to this increase in GMST from preindustrial to present are highlighted in blue (orange). The 95% confidence intervals are shown in brackets.

Time period (data type)		**Probability ratio** (95% confidence intervals)	**Intensity change (%)** (95% confidence intervals)
Past-Present	Observations	3.19 (0.0019 to 10^8)	1.34 (-43.1 to +73.4)
	Models	1.96 (0.20 to 51.3)	8.28 (-12.8 to +32.6)
	Synthesis (weighted)	2.00 (0.13 to 290) *	7.40 (-19.4 to +40.3) *
	Synthesis (unweighted)	2.50 (0.01 to 10^6)	4.81 (-32.2 to +57.2)
Present-Future	**Models only**	1.55 (0.55 to 3.86)	4.45 (-4.71 to +13.6)

Table 5: Summary of results for events like Typhoon Odette in the June-December period due to warming of 1.2 °C, corresponding with the synthesis bars shown in Fig. 8. Increases (decreases) in likelihood and intensity due to this increase in GMST from preindustrial to present are highlighted in blue (orange). The 95% confidence intervals are shown in brackets.
**The main results reported for the current section.*

https://doi.org/10.5194/egusphere-2025-6337
Preprint. Discussion started: 3 February 2026

For extreme rainfall events in December, the synthesised observations and climate models respectively give differing trends related to anthropogenic warming. While observations estimate a strong but highly uncertain increase of around a factor of 100 (0.02 to 10^9) in the likelihood and of 58% (-20 to +214%) in the intensity of such events, climate models suggest a weak decrease by a factor of approximately 0.83 (0.02 to 22.8) in likelihood and 2% (-31 to +38%) in intensity, consistent with no significant change (table 4). The synthesised result drawing on both lines of evidence gives an approximate increase in the likelihood by a factor of 1.22 (0.014 to 301) of such events, and an increase in intensity of 8% (-30 - +67%). This is suggestive of an increase in line with Clausius-Clapeyron scaling and is broadly in agreement with the conclusion of section 2, though is not significant at the 95% confidence level. This synthesis is weighted more heavily upon the model estimate due to the smaller statistical uncertainty on this estimate. Due to the strong disagreement on the strength of change between the two lines of evidence, we also consider the unweighted synthesis result, giving equal weight to observations and models, in determining the likely direction and magnitude of change. The unweighted result shows a strong increase in likelihood, by a factor of 11 (0.01 to 10^6), and in intensity, by 28% (-27 to +114%), though the best estimates themselves are largely illustrative given the wide uncertainty ranges. Overall, given the strong increase in observations relative to models, it is reasonable to conclude that anthropogenic warming has resulted in an overall increase in such extreme December rainfall events, though there is very significant uncertainty on quantifying this effect.

Confidence is higher for extreme rainfall events occurring across the wider TC season of June-December (table 5). Specifically, at present levels of anthropogenic-induced warming compared to preindustrial times, the best estimate of the change in likelihood for events of similar intensity to Odette in June-December is a factor of 2 (0.13 to 290), and the increase in intensity of events of similar likelihood to Odette in June-December is around 7% (-19% to +40%) (table 5). Given the agreement between observations and models, and agreement with the circulation analogues methods in section 2, confidence is high in reporting these weighted estimates rather than the more conservative unweighted results and associated range, though this also suggests an increase in likelihood by a factor of 2.5 (0.01 to 10^6), and in intensity by 5% (-32 to +57%).

We combine this evidence with that from other attribution studies, as well as the estimates of further intensification with future warming (Tables 4 & 5, Figs. B6 & B7), circulation-based analysis in Sect 2 using different data sources, and physical understanding of intensifying short duration precipitation extremes in a warmer atmosphere. Collectively, this evidence suggests that extreme rainfall associated with typhoons such as Odette across the typhoon season striking the southern central Philippines are becoming more frequent due to ACC, and the likelihood of extreme rainfall such as that equal to or exceeding that from Odette has doubled (between a factor of 0.13 and 290, with 95% likelihood) due to ACC, with intensity increased by an amount approximately in line with Clausius-Clapeyron scaling of 7% (-19% to +40%).

Clearly, accurately quantifying the changes in extremes is challenging even when the direction of change is known, given the high uncertainties. The results presented in this section are not statistically significant at the 95% level for a range of reasons.

https://doi.org/10.5194/egusphere-2025-6337
Preprint. Discussion started: 3 February 2026

Primarily, the shortness of data records. The gridded products used here mostly begin around 1980, except for ERA5, which naturally leads to higher sampling uncertainty and requires a greater extrapolation of the trend with GMST. In addition, the relative scarcity of in-situ weather stations means that satellite data is relied upon more in the region. Furthermore, the limited accessibility of individual weather station data series has directly hindered the ability of this study to validate the products used. The high uncertainty on the observational estimates is especially prevalent for June-December in which individual observations disagree on the sign of change. In this situation, the longest running dataset, ERA5, gives an increase across both metrics, increasing our confidence in the synthesised result of an overall increase. Additional work using complementary methods is required to assess changes in intensity and likelihood of such storms alongside the work presented in this section. For instance, accounting for sources of natural variability by incorporating additional covariates into the statistical models used, exploring changes during the wider 'less active season' from November to March in which Odette occurred, and disentangling the influence of ACC on other drivers such as the sea surface temperatures and atmospheric conditions in which the storm developed.

4 Attribution of extreme wind speeds using a synthetic tropical cyclone model (IRIS)

4.1 Data and methods

Assessing changes in tropical cyclone (TC) intensity due to climate change remains a challenge for several reasons. First, observational records are only reliable since approximately 1980 and underwent a step-change in the satellite era. Second, TCs are rare in any given location. Third, modelling the wind speeds of the most intense cyclones requires high spatial resolution (< 10 km), which are computationally expensive and thus ensembles of such models are too small to capture changes in rare events. To overcome these challenges, here we use a new global tropical cyclone wind model (IRIS, Sparks and Toumi, 2025, 2024).

This model is based on several robust principles in TC theory, simulating the decay from the point of lifetime maximum intensity (LMI). The LMI and where it occurs is a key determinant of the wind speed at landfall. The LMI is governed by atmospheric conditions through the potential intensity (PI), which gives a theoretical maximum intensity for a TC based on the atmospheric temperature and humidity vertical profiles, and sea surface temperatures. Observations show that the relative intensity, defined as observed maximum intensity divided by the PI, follows a robust uniform distribution. This drives the stochastic model lifetime maximum intensity. The landfall intensity is then a fraction of this lifetime maximum intensity depending on the time to landfall. Observed historical TC tracks between 1980 and 2021 from the IBTrACS database are stochastically perturbed by the model to create 10,000 years of synthetic TC tracks. Explicit model description and additional details can be found in the IRIS model description paper (Sparks and Toumi, 2024).

https://doi.org/10.5194/egusphere-2025-6337
Preprint. Discussion started: 3 February 2026

At the time of Odette, the global mean temperature was ~ 1.2 °C above pre-industrial temperature (Fig. 10a). The anthropogenic trend is assumed to be the global zonal mean PI trend, removing potential model biases and regional-scale variability, and use the observed PI trend since 1979 from ERA-5. To estimate the pre-industrial PI state, we extrapolate backwards the current observed trends from 1979 to present (Fig. 9). This approach avoids the need for any specific climate model and is therefore both simple and robust.

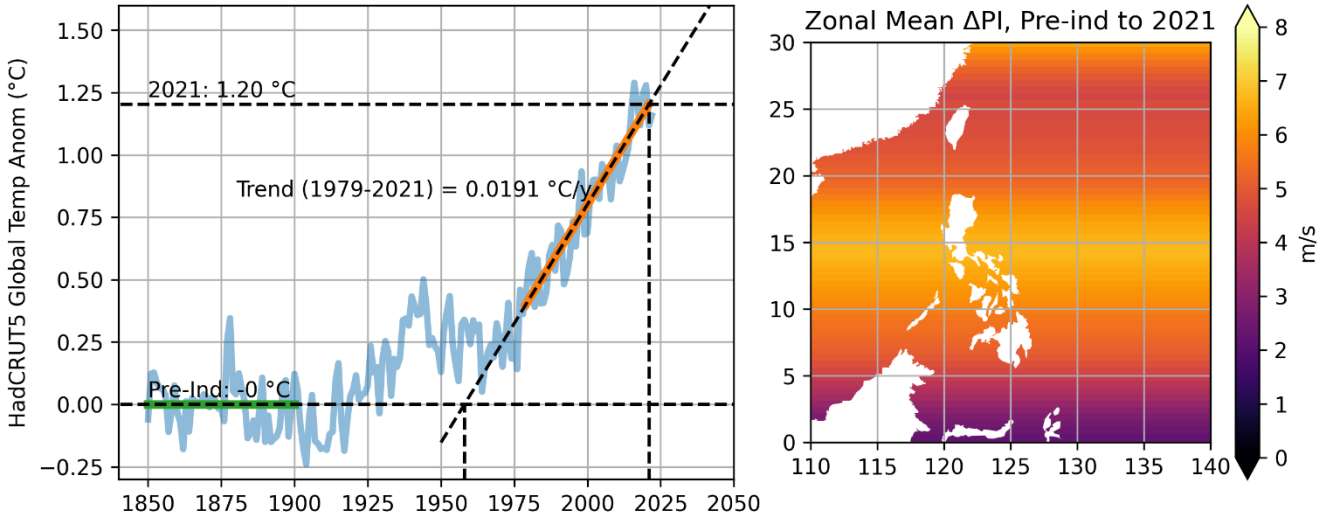

Figure 9: a) Global mean surface temperature showing the scaling method. The 2021 warming is +1.20 above pre-industrial, which is defined as the period 1850-1900. The warming trend between 1979-2021 (the ERA5 period) is +0.0191 °C/yr. b) Zonally averaged PI change from the pre-industrial baseline to 2021 over the western Pacific region using ERA5.

We split the Philippines into three "Gates" based on the landfall climatology: North (0), Central (1) and South (2). Odette made landfall at the southern edge of zone 1 (Fig. 10). The numbers of landfalling events and their intensities at landfall are tallied, enabling the construction of return curves (Fig. 10). From this, the likelihood of a landfalling event at category 5 can be estimated under both current and preindustrial conditions. This in turn enables estimation of the fractional attributable risk (FAR), given by

$$FAR = 1 - \frac{P_0}{P_1}, \quad (1)$$

Where P_1 and P_0 are the probabilities of event occurrence in the current and preindustrial climates, respectively. We note that the basin-scale spatial distribution of the model tracks is conditioned by the observed tracks. As such, if the basin-scale distribution climatology is misrepresented in the observation period (e.g. due to uneven sampling of internal climate variability

https://doi.org/10.5194/egusphere-2025-6337
Preprint. Discussion started: 3 February 2026

states) then it will be reproduced in the model. This in turn may affect local return period estimates. However, we would still expect the resultant FAR/probability ratio in different climate periods to be robust. Furthermore, we minimise the effect of internal climate variability on the PI change, and consequently the resultant FAR, by using a zonally averaged trend over several decades to drive the model.

4.2 Results

For the all-Philippine landfall for a Category 5+ wind speed, IRIS estimates a return period of 2.6 years in 2021 compared to a pre-industrial value of 4.4 years (Fig. 10). This corresponds to an increase in likelihood of approximately 70%, or equivalently a FAR of about 0.39 (equation 1). In addition to this probabilistic framing, there is an equivalent interpretation of this analysis on the attributable change in intensity. The wind speed of a typhoon with a return period of 2.6 years has increased by approximately 5 m/s from pre-industrial to 2021. This result agrees with other attribution analysis for typhoons in the region using a pseudo-global warming approach (Delfino et al., 2023). This wind speed increase is close to the uncertainty of measurements and would not be detectable through observational analysis alone.

If we instead consider the return periods at the three Gates 0,1 and 2, then the FAR is 0.43, 0.34, and 0.28, respectively. The increased risk with increased latitude can be understood by the similar latitude pattern of PI change (Figs. 9 & 10). Given the larger sample size for the all-Philippine landfall dataset, this is the most robust FAR result i.e. about 0.4. For the more specific location at Odette's landfall, IRIS suggests that a fractional attributable risk of about 0.3 (between 0.34 and 0.28, Gate 1 and 2 respectively) may be reasonably considered but is not as statistically robust as the all-Philippine result. Given that it is always possible to specify with greater granularity the specific event domain (e.g. tailoring the 'Gate' to an area just around the exact landfall), selecting an event definition is a compromise between relevance to the event itself and statistical power gained from a larger sample size. We conclude that the all-Philippines region (with FAR ~ 0.4) is the best compromise between these factors, as it provides both a large sample of events and risk-relevant information for storms like Odette across the nation. The current return period in the individual gates is in the range of 14 to 41 years, which is comparable to that found for rainfall (Table 5). To give an uncertainty range on the estimates of FAR, independent 120-year samples, representing the approximate duration of the historical period between present and preindustrial warming levels, are drawn from the wider 10,000-year simulation. This enables determination of the probability distribution of FAR (Fig. C1), returning a 95% confidence interval of 0.03 to 0.66. The standard error of the best estimate mean, 0.39, is 0.015, or less than 4%.

https://doi.org/10.5194/egusphere-2025-6337
Preprint. Discussion started: 3 February 2026

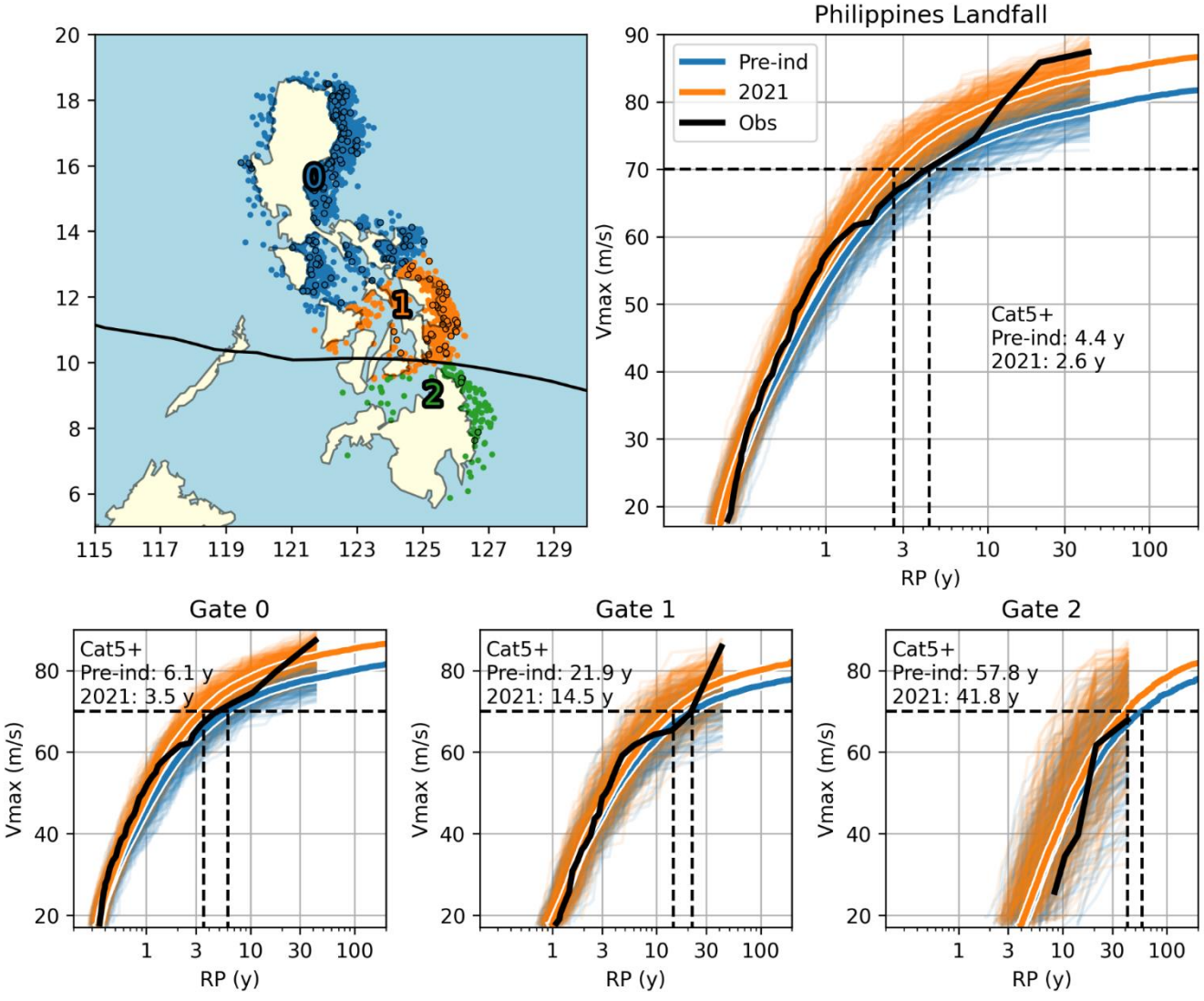

Figure 10: a) Observed (black circles) and IRIS (coloured dots) landfall events in the Philippines. Observations are IBTrACS (1980-2021). IRIS events are drawn from a sample of 420 years. Landfall events are categorised by location into north (blue, gate 0), central (orange, gate 1) and south (green, gate 2). The black line shows the path of Odette. b-e) Return period curves for all-Philippines landfall events, and landfall events in gates 0, 1 and 2. The IBTrACS 1980-2021 observations are shown in black and 10,000-year IRIS simulations are shown in blue (pre-industrial climate conditions) and orange (2021 climate conditions). Ensembles of 42-year samples of IRIS output, equivalent to the duration of the IBTrACS period, are shown in fine lines. Dashed lines show return periods of Category 5 events (70 m/s) in IRIS simulations.

https://doi.org/10.5194/egusphere-2025-6337
Preprint. Discussion started: 3 February 2026

5. Discussion and conclusions

In this section, the results of meteorological hazard attribution are summarised and the implications of this for the damages from Typhoon Odette that are attributable to ACC are discussed. In particular, the FAR statistic (Sect. 4) is employed to compare and combine results from the hazard assessments in sections 3 & 4. The circulation analogues analysis in section 2 does not provide a probabilistic assessment of hazards and is therefore not combined in the quantitative conclusions of this study. However, the estimated change in intensity of extreme rainfall was broadly in line with the result from section 3, which is used as an additional qualitative line of evidence in the conclusions of this study.

The probability ratios estimated for the multiple meteorological hazards from Odette due to anthropogenic climate change are as follows. In Sect. 3, we found that extreme rainfall totals from TCs like Odette have become about 2 times (or 100%) more likely, with an uncertainty range of 0.13 to 290, due to anthropogenic climate change. In Sect. 4, the wind speeds from category 5 TCs were found to occur around 70% more often, with an uncertainty range of 3 - 200% more, due to anthropogenic climate change. Using equation 1, this gives best estimate values of FAR of 0.50 (-0.87 to 0.997) for rainfall and a FAR of 0.39 (0.03 to 0.66) for wind speed. Table 6 shows this range of values across all hazards, event definitions and synthesis methods, calculated using the best estimates and lower and upper bounds of the probability ratios.

Hazard (event definition)		FAR (95% confidence interval)		
		Best estimate	Lower bound	Upper bound
Rainfall	June-December (weighted)	0.50*	-0.87	0.997
	June-December (unweighted)	0.60	-0.99	~1
	December (weighted)	0.18	-0.986	0.997
	December (unweighted)	0.91	-0.989	~1
Winds	All-Philippine	0.39*	0.03	0.66
	Gate 0	0.43		
	Gate 1	0.34		
	Gate 2	0.28		

https://doi.org/10.5194/egusphere-2025-6337
Preprint. Discussion started: 3 February 2026

*Table 6: Estimates of the FAR for each hazard associated with Odette, for each event definition and synthesis method, alongside uncertainties. All negative values are given by the inverse FAR, as in equation (1) but with P_1 and P_0 inverted. *The best estimates for each hazard.*

5.1 Using the Fractional Attributable Risk

Using the FAR to attribute damages from an event requires careful interpretation and involves several conditions. First, the FAR statistic is asymmetric in nature, ranging between an upper bound of 1 (an event was impossible without ACC), to negative infinity (an event made impossible by ACC). The central estimate of 0 represents no change due to ACC, positive values (0-1) showing a quantifiable increase due to ACC and negative values (< 0) show a quantifiable decrease. As a result of this asymmetry, which arises because FAR assumes an increase in likelihood between P_0 and P_1 (equation 1) only FAR values of 0-1 are applicable to the estimation of attributable impacts. We therefore use the inverse FAR statistic (equation 1 with P_0 and P_1 inverted) for decreasing likelihoods and a negative sign to represent the corresponding fractional attributable decrease in risk (given by negative values in Table 6).

For rainfall, all FAR results are highly uncertain as the confidence interval encapsulates no change in likelihood (FAR=0), making them statistically insignificant at the 95% level (Table 6). However, statistical significance alone is not sufficient to dismiss a hypothesis in the presence of other relevant evidence, and an overreliance on these uncertainty ranges risks type II errors in which the influence of climate change is falsely dismissed (Shepherd, 2019). Given the relatively short length of data records, it is expected that natural variability would result in a wide uncertainty range, especially for the December-only event definition (which includes plausible best estimate probability ratios of both 11 and 1.22; table 6). Furthermore, as shown in Sect. 3, multiple event definitions give similar results and this result aligns with physical understanding, both of which reinforce confidence in the accuracy of these results. Consequently, confidence is high that anthropogenic climate change intensified the rainfall of Odette, with the best estimate yielding a doubling of the likelihood of such intense rains. Meanwhile, confidence is high both quantitatively and qualitatively that ACC increased the wind speeds of Odette, as the all-Philippines result is statistically significant, best estimate results are positive across all 'Gates', and the underlying method is based on physically robust potential intensity theory.

Second, the FAR is probabilistic in nature. This statistic has been used in several attribution studies, including TCs and other extremes, to estimate attributable damage. For example, rainfall from Typhoon Hagibis was increased in likelihood by 67% (15-150%); the resultant best estimate FAR of 0.4 led to an estimate of US$4 bn in attributable damages from the total damages of US$10 bn (Li and Otto, 2022). Hurricane Harvey rainfall was found to have increased in likelihood by a factor of around 4 across multiple studies, giving FAR=0.75 and an estimate of attributable damage of US$67 bn (Frame et al., 2020).

The key message in such cases is that the "[probability] ratio can be interpreted as a lower bound to relative changes in the expected losses due to the extremes provided that the consequences of extreme events of a fixed intensity do not decrease with

https://doi.org/10.5194/egusphere-2025-6337
Preprint. Discussion started: 3 February 2026

warming, consistent with expectations" (Kharin et al., 2018). In essence, over a long period at the current level of warming, the losses due to events of at least the magnitude of the event in question would be a factor of the probability ratio larger than those due to the same class of events in preindustrial times. Using equation 1, the FAR is then used to quantify attributable damage related to this change in risk of the most extreme events.

More broadly, the FAR is valid for a class of events to which the event belongs, which also includes events at least as intense as that event. In general, it is not a direct attribution of damage from a single event but attributes a level of impact from events of at least the given intensity. The other way to attribute damage from specific extremes within the same framework involves using a relative magnitude framing (Perkins-Kirkpatrick et al., 2022). Within the simplest form of this method, the change in magnitude due to ACC for an event of equivalent frequency is calculated. This is then fed into a 'damage function', returning a level of damage done by events of the same probability in different climates, giving the 'direct' attributable impacts.

The latter framing was not used here for several reasons. Primarily, constructing a damage function (or 'vulnerability curve') from the available disaster data introduces an additional layer of uncertainties; in a recent study that empirically constructed such functions, the uncertainties in this region were particularly large (Eberenz et al., 2021). There is also significant variation in the damage susceptibility across the Philippines, rendering national-scale assessments difficult (Baldwin et al., 2023). It is noteworthy that the eastern Visayas have a significantly larger damage fraction than both the national capital region (surrounding Manila) and the national average for a given wind speed (Baldwin et al., 2023).

While debate continues as to the usefulness of FAR in quantifying the attributable impacts of a specific extreme event, there is a special case for the interpretation of FAR-based impact statements when such events are 'system-breaking'. These events are above a key threshold in magnitude at which impacts rapidly increase. For instance, this could involve the rainfall required for a river to burst its banks, or the wind speeds exceeding the strength of local structures. In this case, the FAR-based approach gives a more direct estimate of damage due to ACC because the frequency of such events is all that determines the total level of impacts. While it is not clear if Odette was 'system-breaking', and the highly uncertain vulnerability curves described above do not inform this, category 5 TCs are known to produce winds beyond the capacity of many structures to withstand. In many regions in which vulnerability curves are more confident, the damage fraction is significantly above 50% for winds of category 5 level (Baldwin et al., 2023). Put simply, for the most intense storms an increasing frequency likely causes an equivalent increase in damage, while comparably small changes in overall magnitude may be of relatively little importance.

As a result of the above arguments, this study uses the FAR-based framing, as it is grounded in the simple logical assertion that more intense and probable hazards result in greater damage than less intense and probable hazards, for a given vulnerability and exposure context. While not tied directly to the magnitude shift of this specific storm, it is part of the same statistical framing and carries an important attribution statement. That is, events at least as intense as Odette, and therefore most likely causing at least as much damage, have become more likely by a given factor (the probability ratio) due to anthropogenic

https://doi.org/10.5194/egusphere-2025-6337
Preprint. Discussion started: 3 February 2026

climate change. And, consequently, an equivalent fraction of the damages of all events within that 'class' can be attributed to its influence through the FAR.

5.2 Attributable Impacts of Typhoon Odette

The impacts of TCs often result from a combination of several compounding meteorological extremes. This includes rainfall that may lead to flash and riverine flooding and mass movements such as landslides and mudslides, and extreme winds that lead to direct destruction of property and infrastructure as well as indirect damage through causing storm surges, which further lead to coastal flooding. During a TC, it is the combination of these factors that lead to such devastation, as each heightens the regional vulnerability to other concurrent hazards, resulting in a non-linear amplification of impacts. The assessments conducted in sections 3 and 4 are for rain and wind hazards in isolation. However, since both are increasing in parallel, it is likely that their combined attributable increases made the damages disproportionately larger than either their individual contributions or their sum.

This has two implications for this study. First, it reinforces the choice to use a FAR based approach to damage attribution given the insurmountable challenge not only in constructing vulnerability curves, as described above, but in disentangling the relative role of each type of hazard. Second, in line with compound events attribution theory, the influence of ACC on the combined impacts of Typhoon Odette – the bivariate FAR – is a function of both its influence on each of the hazards in isolation, given by the univariate FARs, and the correlation between hazards (Zscheischler and Lehner, 2022).

Within this study, it is impossible to directly assess the joint changes in rainfall and high winds because they are modelled using different methods. For many compound events, such as concurrent heatwaves or droughts in different breadbasket regions, or individual droughts consisting of both heat and a lack of rainfall, it is not always intuitively clear how strongly the phenomena are correlated. However, for TCs the two phenomena in question are highly correlated. This was tested using the ERA5 and MSWEP/MSWX datasets (Fig. D1). Within these datasets, the June-December maximum rainfall used in the trend analysis in section 3 and the maximum and average wind speeds on the same dates each have a Pearson correlation coefficient of ~0.64 (p values approximately 10^{-9} and 10^{-6}, respectively), confirming that there is indeed a strong positive correlation. That in turn suggests that the following criterium, derived empirically through case studies using several climate models, is met in this case: "if variables are strongly correlated and have similar trends, the bivariate FAR is at the upper range of the univariate FARs" and "both variables have similarly large trends or the dependence between both variables is weak, bivariate FARs are larger and are likely to provide a more adequate quantification of the anthropogenic influence" (Zscheischler and Lehner, 2022).

This means that the overall FAR for the combined extremes of Odette, which is most pertinent to the damages experienced, is most likely equal to or slightly greater than that for the larger of the univariate FAR statements. This suggests a best estimate of FAR >= 0.5 related to the compounding winds and rainfall Odette, suggesting that the risk of similar impacts has likely

https://doi.org/10.5194/egusphere-2025-6337
Preprint. Discussion started: 3 February 2026

more than doubled due to ACC. However, without further work within a consistent modelling framework it is challenging to be precise or to quantify the uncertainty on this estimate. For risk assessment and adaptation, the individual probability ratios (or FARs) are more robust, though their combined effects and the potentially compounding effect of ACC should not be neglected.

Competing Interests

The authors declare no competing interests.

https://doi.org/10.5194/egusphere-2025-6337
Preprint. Discussion started: 3 February 2026

Appendices

A. Section 2 figures

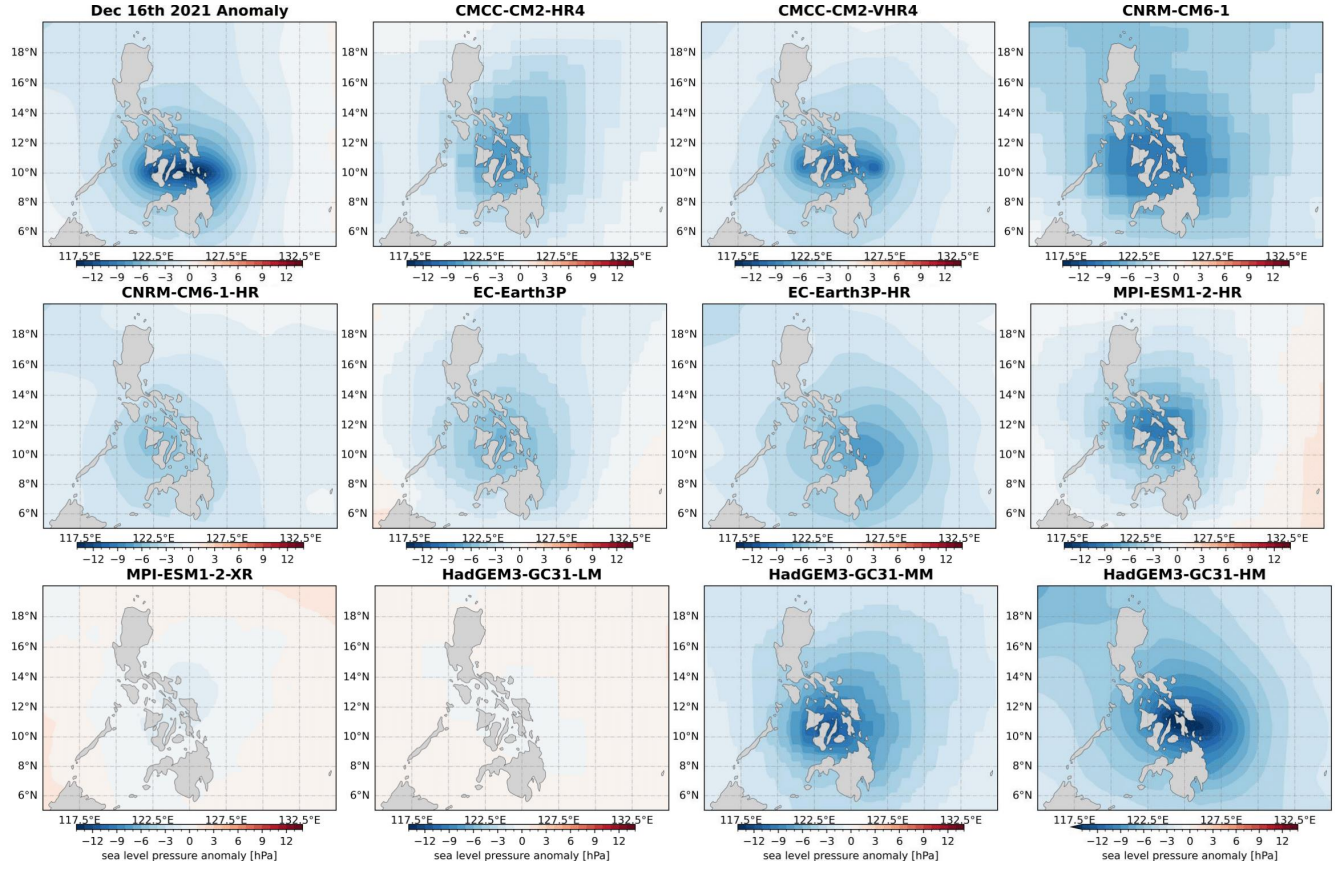

Figure A1: For each model, the sea level pressure anomaly patterns over (5-20 °N,115-135 °E), with the highest spatial correlation to Dec 16th 2021 during Odette landfall is shown.

https://doi.org/10.5194/egusphere-2025-6337
Preprint. Discussion started: 3 February 2026

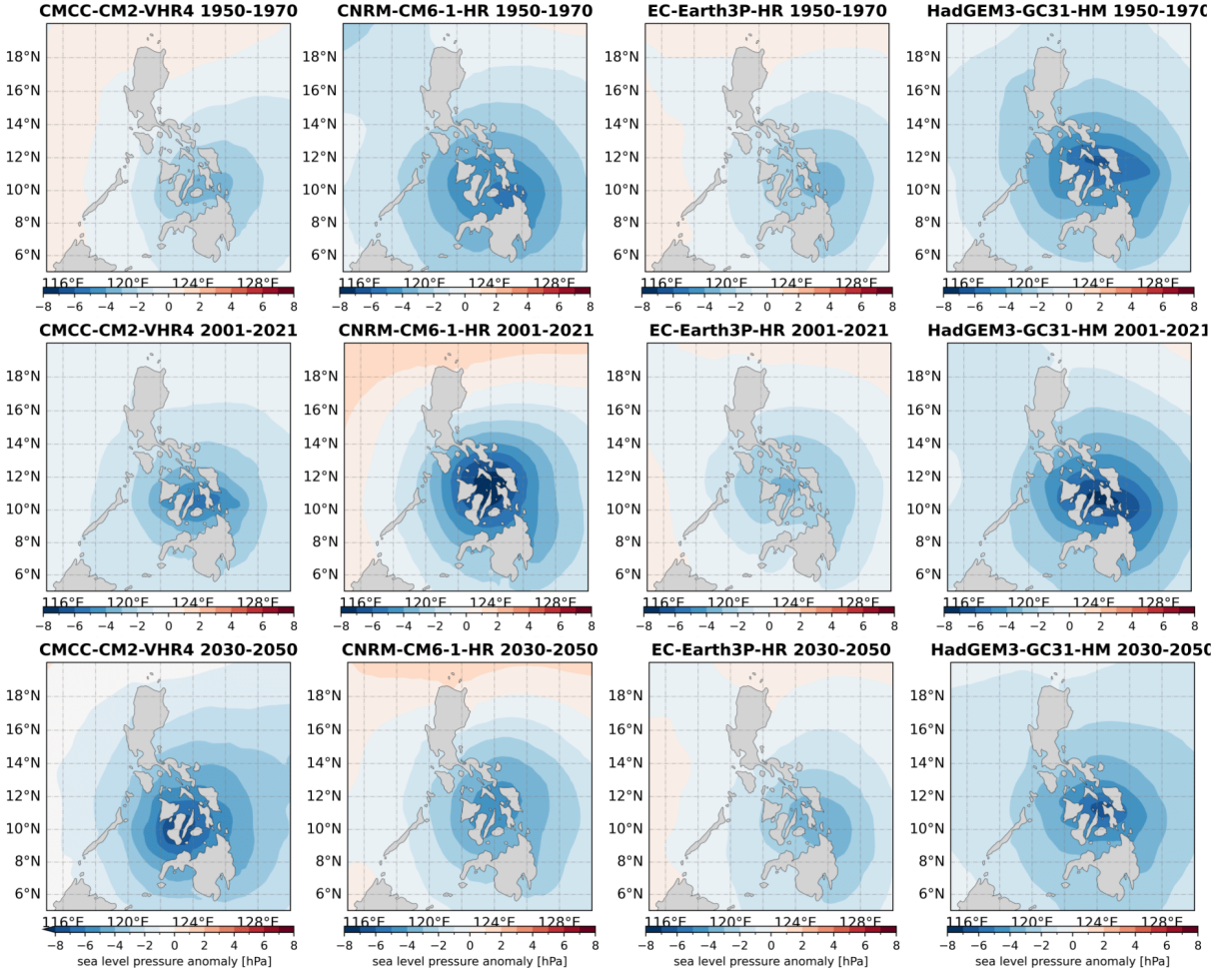

Figure A2: Composite SLP anomaly maps of the top 5 ranking analogues for each of the selected models (rows) and each period past (top), present (middle) and future (bottom).

B. Section 3

B.1 Statistical methods

B.1.1 Observational attribution

https://doi.org/10.5194/egusphere-2025-6337
Preprint. Discussion started: 3 February 2026

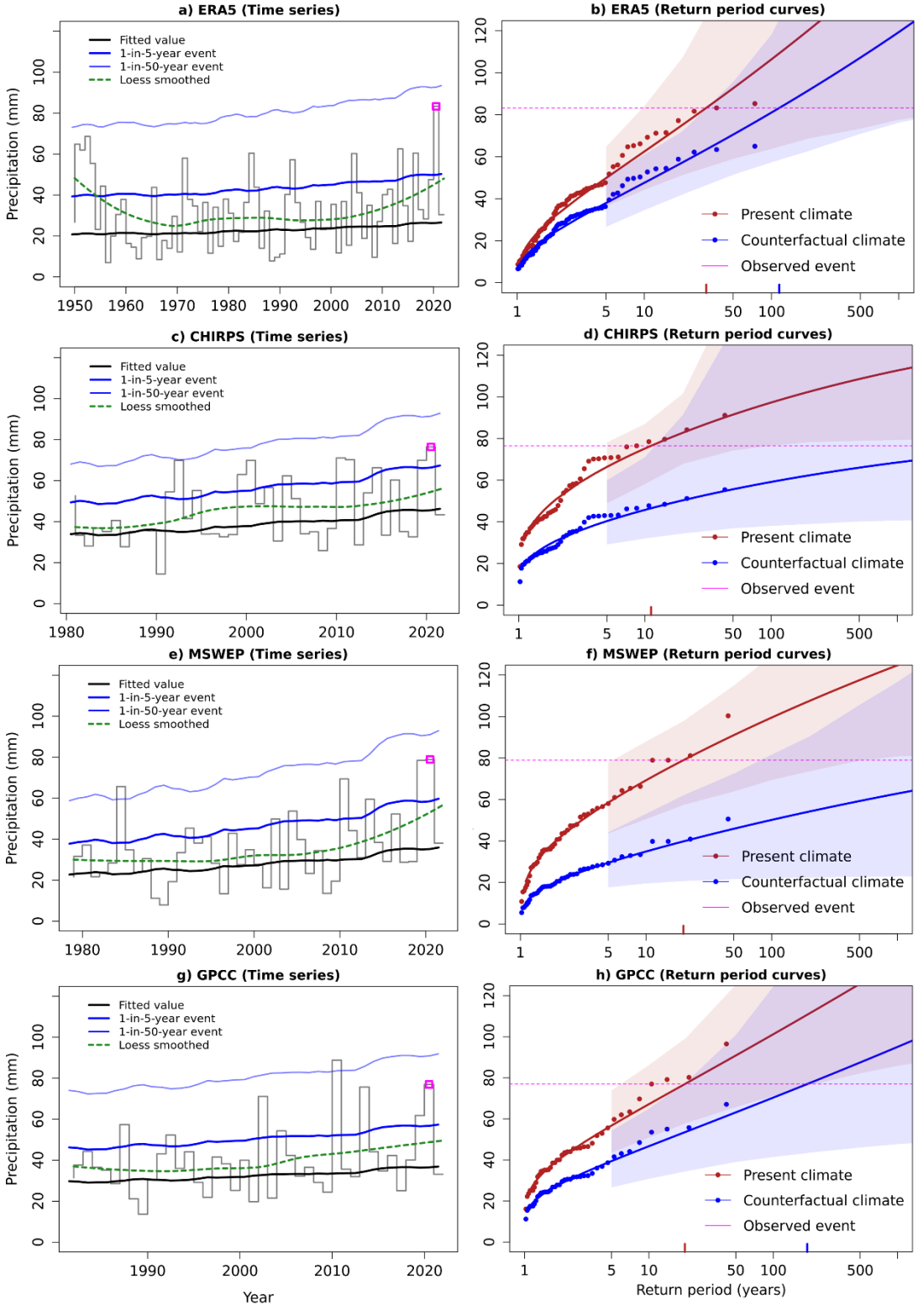

https://doi.org/10.5194/egusphere-2025-6337
Preprint. Discussion started: 3 February 2026

Figure B1: Times series and statistical fits in the four observational datasets, ERA5, CHIRPS, MSWEP and GPCC for December. a) Shows the time series (grey) and fitted statistical model trend (black), with the event associated with Odette highlighted in purple. The modelled 5- and 50-year events are shown as dark and light blue lines, respectively, and the loess smoothed trend is shown by the green dashed line. b) Shows the GEV fit to the ERA5 data at two levels of the covariate GMST: in 2021 (red curve) and in a 1.2 °C cooler climate (blue curve). The dashed purple line shows the magnitude of Odette. The small blue and red lines on the x axis show the estimated return period of the event in the preindustrial and present climates, respectively. c) and d), e) and f), g) and h): As in (a) and (b) for CHIRPS, MSWEP and GPCC data.

https://doi.org/10.5194/egusphere-2025-6337
Preprint. Discussion started: 3 February 2026

B.1.2 Model evaluation

Model / Observations	Seasonal cycle	Spatial pattern	Dispersion	Shape parameter	Event magnitude (mm)
CHIRPS			0.34 (0.191 … 0.412)	-0.147 (-0.594 … 0.574)	83.26
ERA5			0.566 (0.483 … 0.624)	0.066 (-0.187 … 0.334)	76.48
GPCC			0.363 (0.26 … 0.428)	0.0264 (-0.24 … 0.285)	78.94
MSWEP			0.465 (0.362 … 0.551)	-0.071 (-0.56 … 0.118)	76.98
Models					**Threshold for 20-year return period event (mm)**
CORDEX-SEA					
CNRM-CM5_r1_RCA4 ()	bad	good	0.453 (0.356 … 0.539)	-0.197 (-0.70 … 0.072)	76.32852
HadGEM2-ES_r1_RCA4 ()	good	reasonable	0.473 (0.345 … 0.565)	-0.077 (-0.291 … 0.135)	87.81494
HadGEM2-ES_r1_RegCM4-7 ()	reasonable	bad	0.275 (0.179 … 0.32)	0.126 (-0.107 … 0.839)	38.63236
HadGEM2-ES_r1_REMO2015 ()	reasonable	bad	0.402 (0.302 … 0.475)	-0.136 (-0.389 … 0.078)	79.96933
MPI-ESM-LR_r1_REMO2015 ()	good	reasonable	0.379 (0.287 … 0.457)	-0.209 (-0.803 … 0.00043)	76.04281
MPI-ESM-MR_r1_RegCM4-7 ()	reasonable	reasonable	0.287 (0.219 … 0.340)	-0.138 (-0.523 … 0.308)	35.30564
NorESM1-M_r1_RegCM4-7 ()	reasonable	reasonable	0.327 (0.258 … 0.459)	-0.114 (-1.13 … 0.138)	35.02233
NorESM1-M_r1_REMO2015 ()	reasonable	reasonable	0.343 (0.226 … 0.432)	-0.147 (-0.429 … 0.181)	86.92025
CORDEX-EAS					
HadGEM2-ES_r1_RegCM4-4 ()	bad	reasonable	0.484 (0.341 … 0.574)	-0.228 (-0.821 … 0.39)	23.46256
HadGEM2-ES_r1_REMO2015 ()	bad	bad	0.533 (0.420 … 0.617)	0.026 (-0.411 … 0.322)	123.707

https://doi.org/10.5194/egusphere-2025-6337
Preprint. Discussion started: 3 February 2026

MPI-ESM-LR_r1_REMO2015 ()	good	reasonable	0.461 (0.342 … 0.574)	-0.332 (-0.680 … -0.139)	103.8969
MPI-ESM-MR_r1_RegCM4-4 ()	reasonable	reasonable	0.404 (0.289 … 0.503)	-0.227 (-0.778 … -0.069)	46.10828
NorESM1-M_r1_RegCM4-4 ()	good	reasonable	0.310 (0.235 … 0.373)	-0.226 (-0.856 … -0.029)	25.95332
NorESM1-M_r1_REMO2015 ()	reasonable	reasonable	0.332 (0.244 … 0.392)	0.062 (-0.185 … 0.274)	101.2148

Table B1: Model evaluation results for rainfall extremes in December in the study region in the southern Philippines. Each row is a single model, coloured by the evaluation ranking: red for 'bad' and orange for 'reasonable'. No models were ranked 'good' in the evaluation. Models ranked 'bad' are not included in the analysis.

Model / Observations	**Seasonal cycle**	**Spatial pattern**	**Dispersion**	**Shape parameter**	**Event magnitude (mm)**
CHIRPS			0.253 (0.185 ... 0.296)	-0.379 (-0.738 ... 0.132)	83.26
ERA5			0.289 (0.229 ... 0.329)	0.079 (-0.116 ... 0.336)	76.48
MSWEP			0.319 (0.239 ... 0.376)	0.022 (-0.245 ... 0.298)	78.94
GPCC			0.285 (0.199 … 0.332)	-0.0062 (-0.347 … 0.427)	76.98
Models					**Threshold for 20-year return period event (mm)**
CORDEX-SEA					
CNRM-CM5_r1_RCA4 ()	bad	good	0.380 (0.293 ... 0.444)	-0.28 (-0.59 ... -0.077)	96.01875
HadGEM2-ES_r1_RCA4 ()	good	reasonable	0.307 (0.199 ... 0.375)	-0.062 (-0.48 ... 0.38)	116.6165
HadGEM2-ES_r1_RegCM4-7 ()	reasonable	bad	0.144 (0.103 ... 0.177)	-0.26 (-0.72 ... 0.14)	61.15176
HadGEM2-ES_r1_REMO2015 ()	reasonable	bad	0.132 (0.102 ... 0.207)	-0.35 (-1.1 ... 0.025)	97.84563
MPI-ESM-LR_r1_REMO2015 ()	good	reasonable	0.184 (0.137 ... 0.225)	-0.067 (-0.38 ... 0.17)	103.6128
MPI-ESM-	reasonable	reasonable	0.194 (0.145 ... 0.231)	0.16 (-0.26 ... 0.55)	75.11458

https://doi.org/10.5194/egusphere-2025-6337
Preprint. Discussion started: 3 February 2026

MR_r1_RegCM4-7 ()					
NorESM1-M_r1_RegCM4-7 ()	reasonable	reasonable	0.250 (0.181 ... 0.325)	-0.32 (-1.1 ... 0.16)	55.74366
NorESM1-M_r1_REMO2015 ()	reasonable	reasonable	0.153 (0.116 ... 0.183)	-0.20 (-0.51 ... -0.012)	90.9818
CORDEX-EAS					
HadGEM2-ES_r1_RegCM4-4 ()	bad	reasonable	0.182 (0.130 ... 0.265)	-0.26 (-1.1 ... 0.13)	50.78031
HadGEM2-ES_r1_REMO2015 ()	bad	bad	0.170 (0.121 ... 0.205)	0.10 (-0.16 ... 0.43)	137.141
MPI-ESM-LR_r1_REMO2015 ()	good	reasonable	0.184 (0.141 ... 0.216)	0.042 (-0.29 ... 0.26)	134.0954
MPI-ESM-MR_r1_RegCM4-4 ()	reasonable	reasonable	0.164 (0.110 ... 0.199)	-0.12 (-0.33 ... 0.12)	51.68393
NorESM1-M_r1_RegCM4-4 ()	good	reasonable	0.157 (0.120 ... 0.189)	-0.11 (-0.51 ... 0.17)	36.24989
NorESM1-M_r1_REMO2015 ()	reasonable	reasonable	0.232 (0.171 ... 0.281)	0.10 (-0.43 ... 0.38)	129.2698

Table B2: Model evaluation results for rainfall extremes in December in the study region in the southern Philippines. Each row is a single model, coloured by the evaluation ranking: red for 'bad' and orange for 'reasonable'. No models were ranked 'good' in the evaluation. Models ranked 'bad' are not included in the analysis.

https://doi.org/10.5194/egusphere-2025-6337
Preprint. Discussion started: 3 February 2026

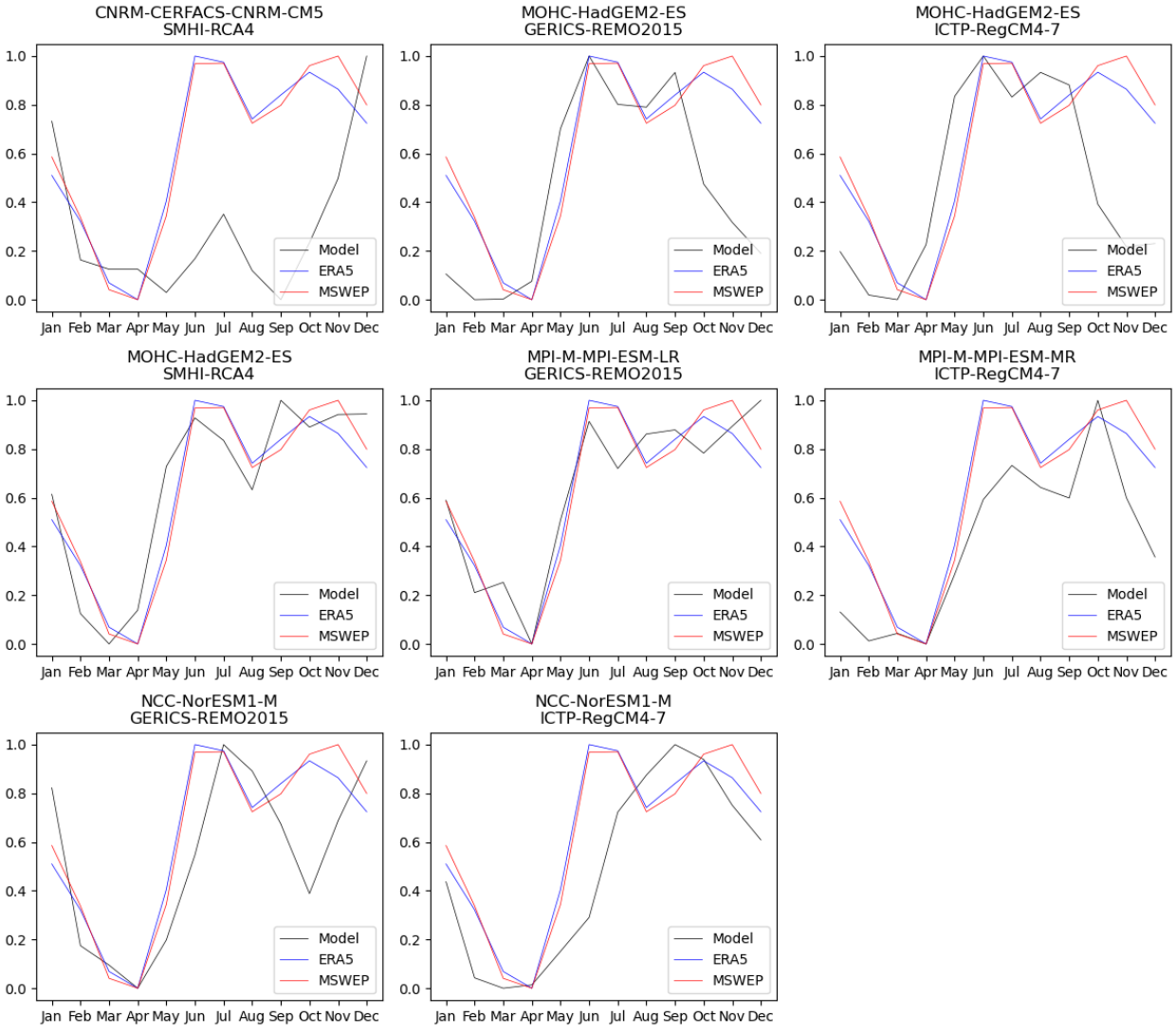

Figure B2: Seasonal cycles of normalised monthly precipitation for the period 1980-2010 in the ERA5 and MSWEP and CORDEX-SEA models.

720

https://doi.org/10.5194/egusphere-2025-6337
Preprint. Discussion started: 3 February 2026

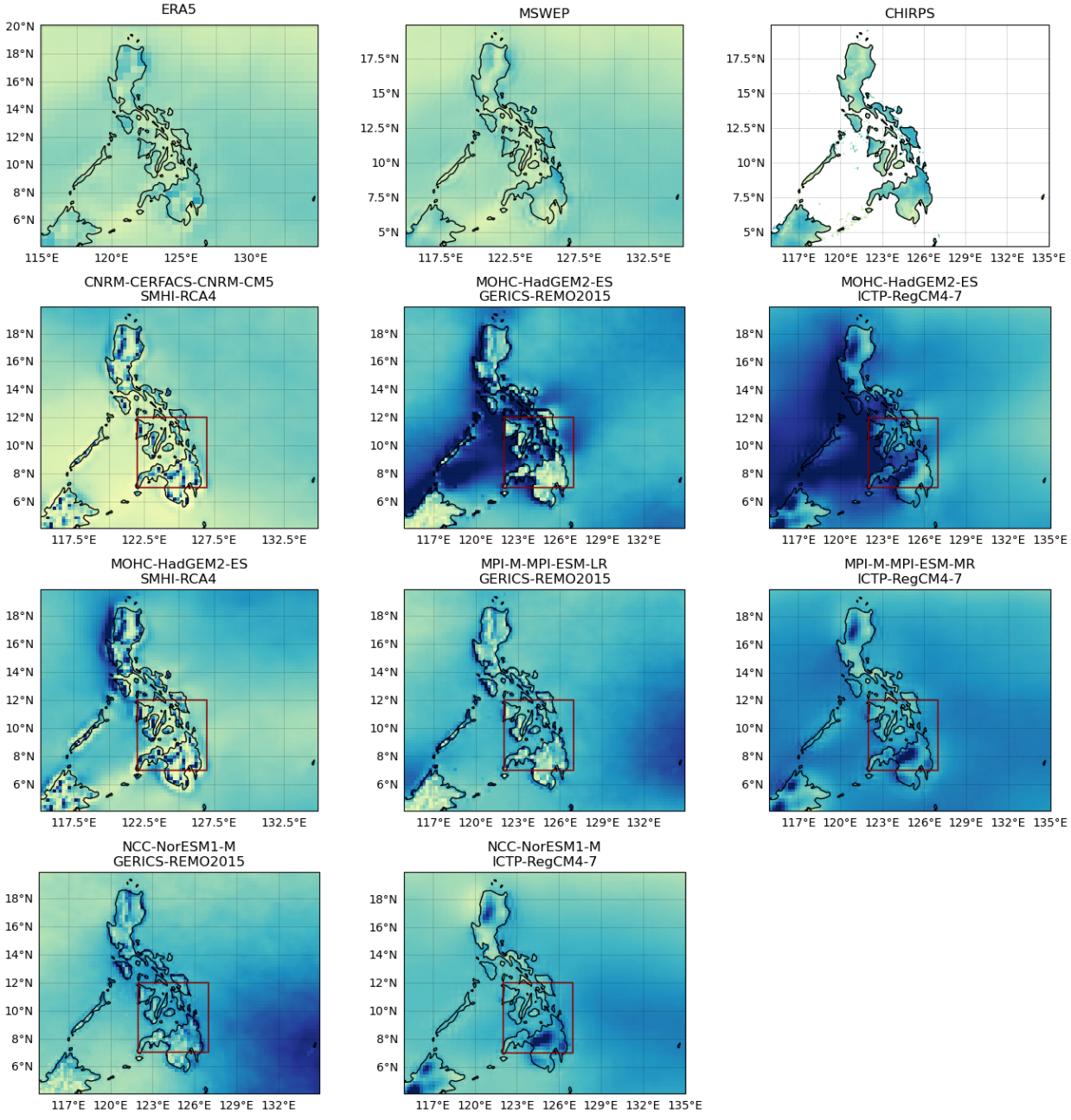

Figure B3: Spatial patterns of mean daily precipitation over the Philippines for the period 1980-2010 in the three highest-resolution observational and reanalysis products and CORDEX-SEA models. The study region is highlighted in red.

https://doi.org/10.5194/egusphere-2025-6337
Preprint. Discussion started: 3 February 2026

760

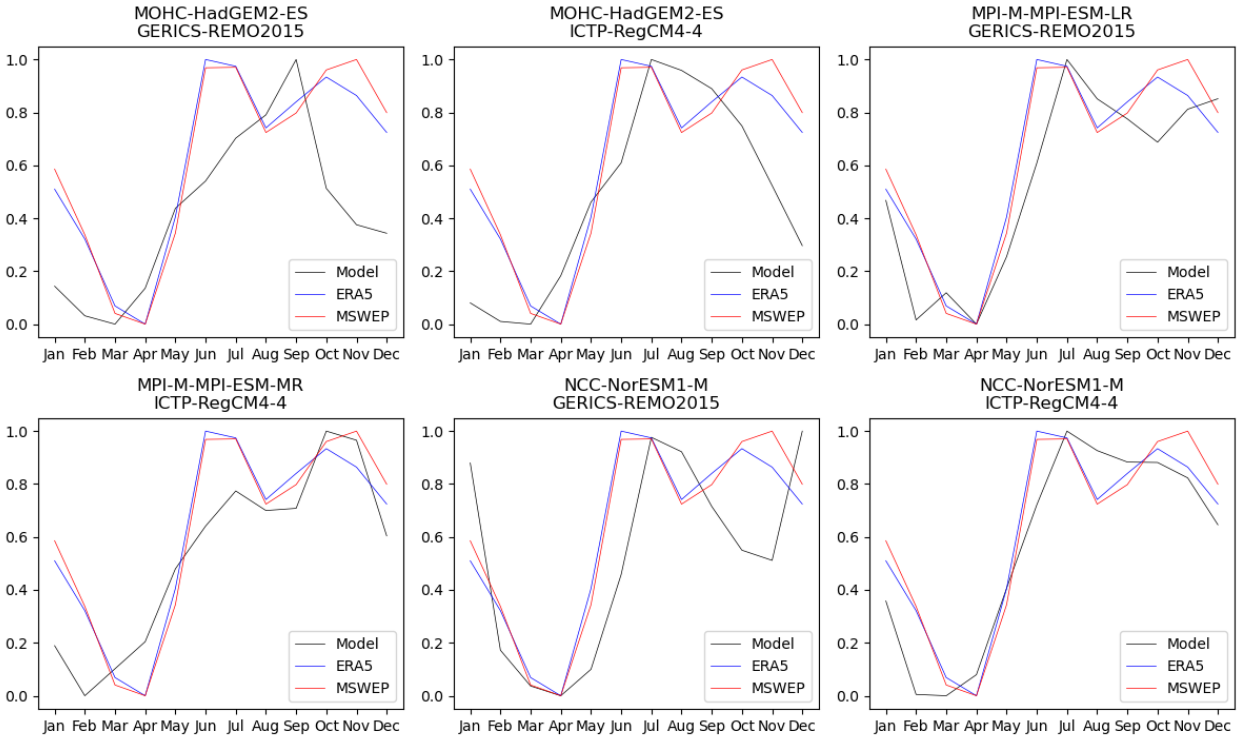

Figure B4: Seasonal cycles of normalised monthly precipitation for the period 1980-2010 in the ERA5 and MSWEP and CORDEX-EAS models.

765

770

https://doi.org/10.5194/egusphere-2025-6337
Preprint. Discussion started: 3 February 2026

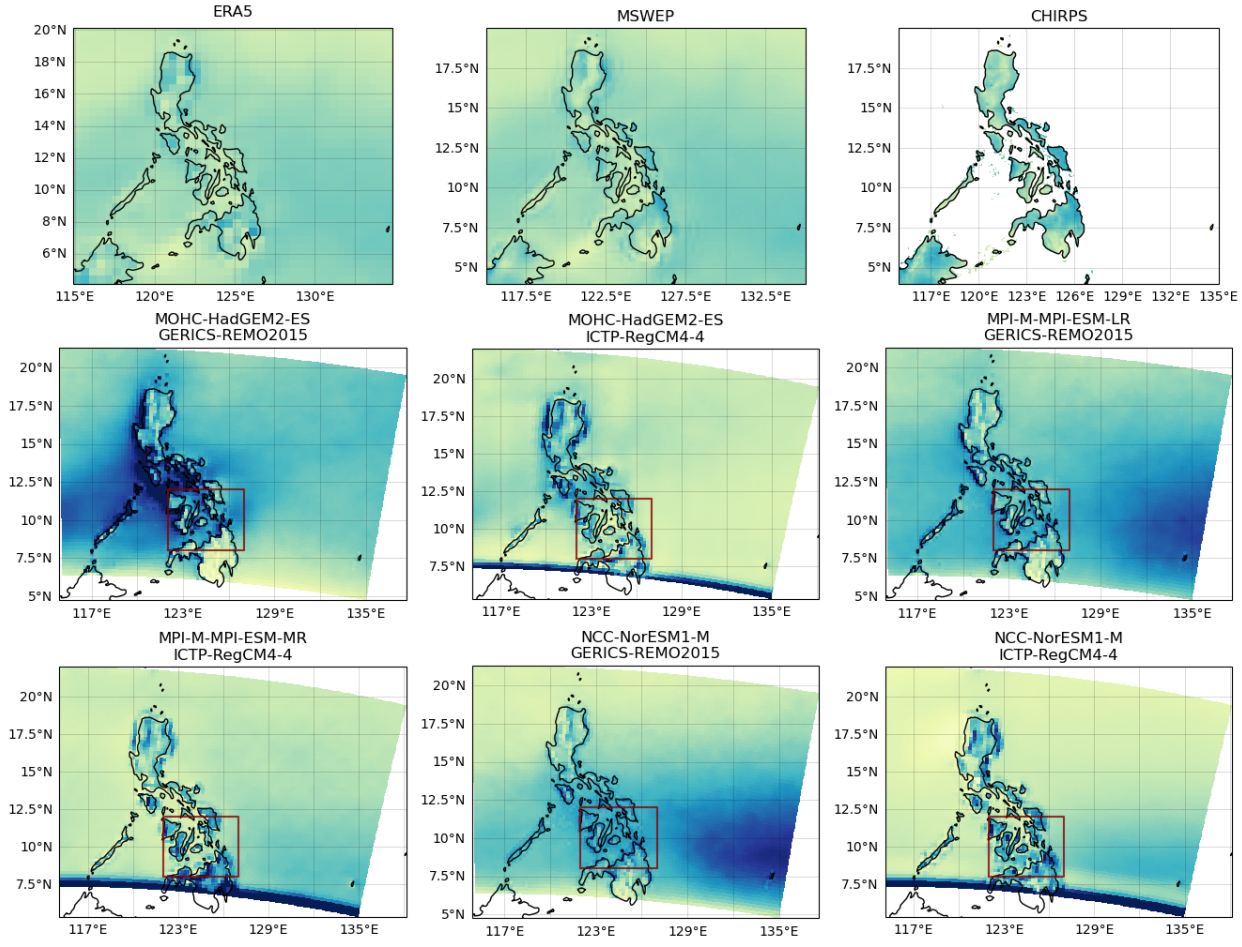

775

Figure B5: Spatial patterns of mean daily precipitation over the Philippines for the period 1980-2010 in the three highest-resolution observational and reanalysis products and CORDEX-EAS models. The study region is highlighted in red. Note: The study region is restricted to a lower bound of 8 °N (rather than 7 °N) to minimise boundary effects.

https://doi.org/10.5194/egusphere-2025-6337
Preprint. Discussion started: 3 February 2026

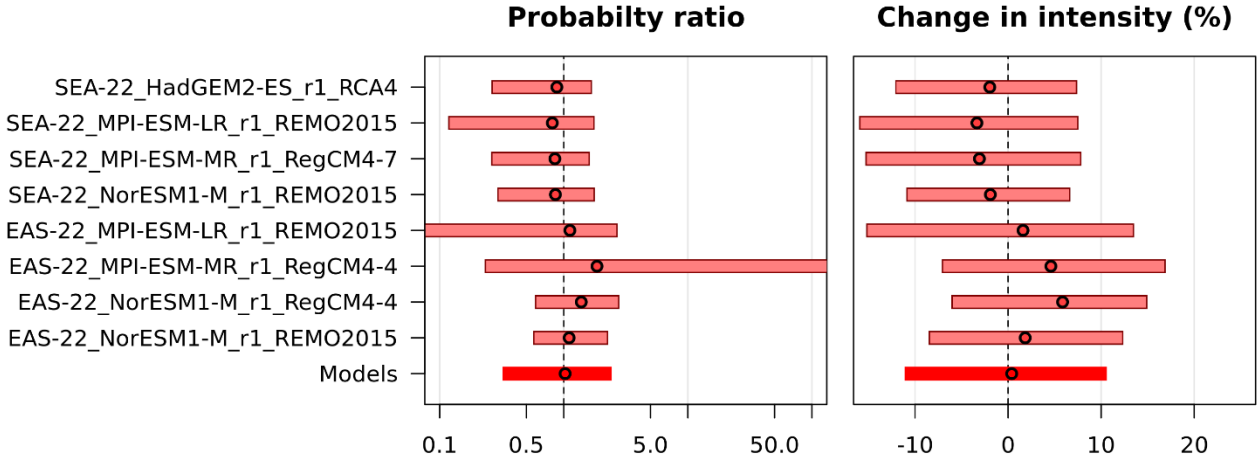

780

Figure B6: Synthesis of (a) probability ratios and (b) intensity changes when comparing the 1-day maximum December precipitation that occurred in 2021 with a 0.8 °C warmer climate (for a total of 2 °C above preindustrial levels).

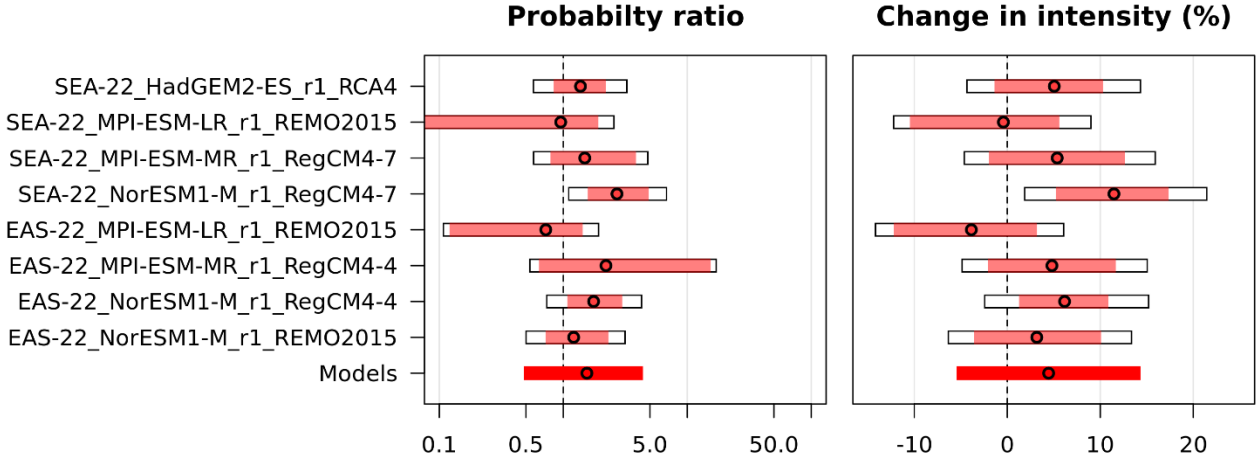

785

Figure B7: Synthesis of (a) probability ratios and (b) intensity changes when comparing the 1-day maximum June-December precipitation that occurred in 2021 with a 0.8 °C warmer climate (for a total of 2 °C above preindustrial levels).

https://doi.org/10.5194/egusphere-2025-6337
Preprint. Discussion started: 3 February 2026

790

C. Section 4

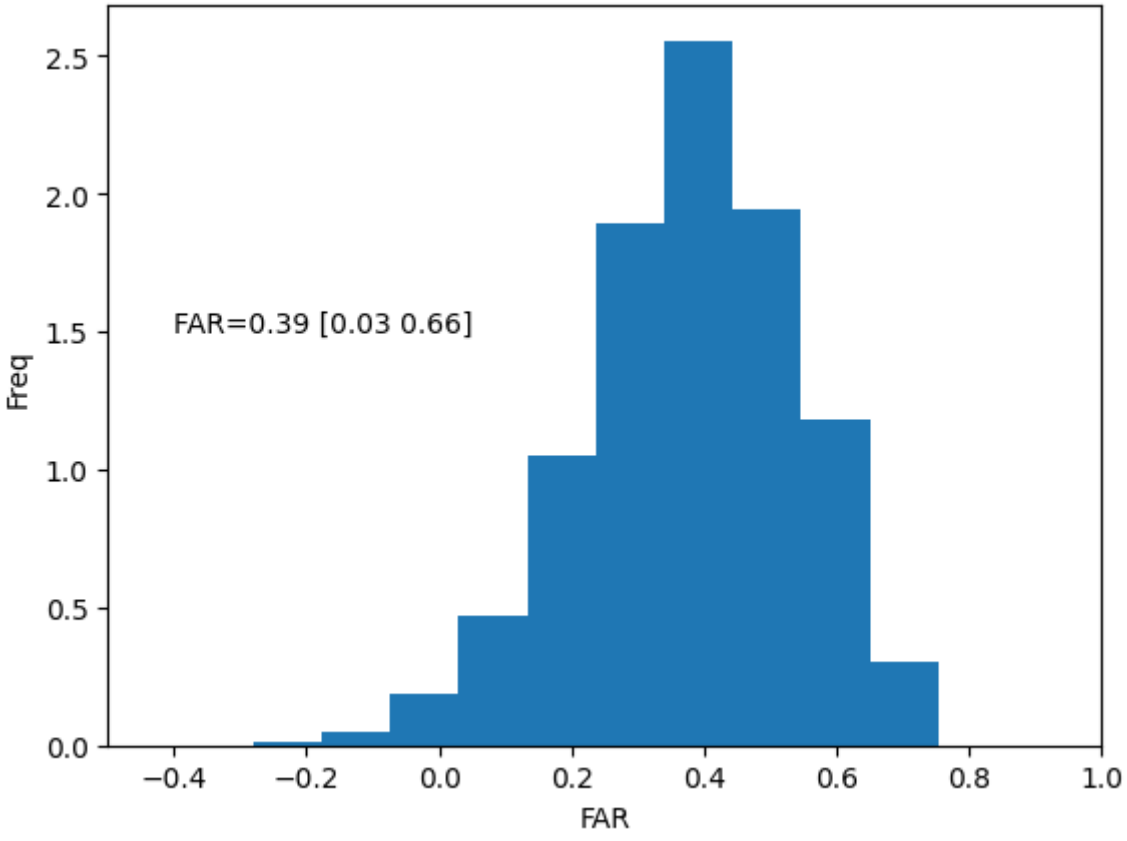

Figure. C1: Probability distribution of 120-year samples of the fractional attributable risk in the 10,000-year simulation,
795 *including the 95% confidence intervals on the best estimate FAR value.*

https://doi.org/10.5194/egusphere-2025-6337
Preprint. Discussion started: 3 February 2026

D. Section 5

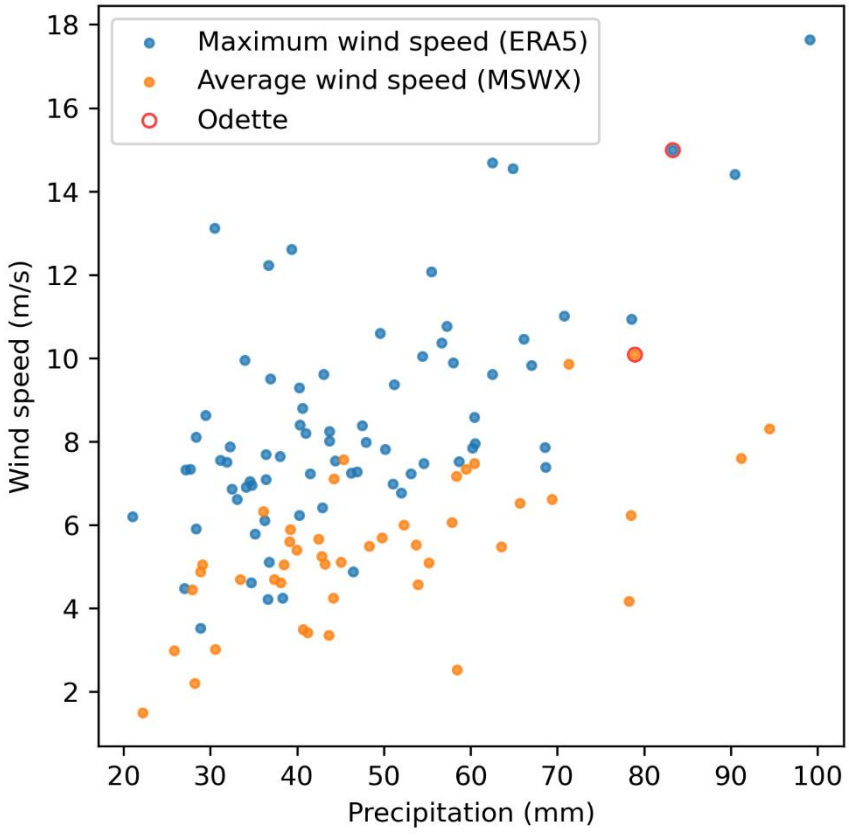

Figure D1: Joint distributions of extreme daily precipitation used for trend analysis in section 3 with daily maximum wind speeds (blue) and daily average wind speeds (orange). Maximum wind speeds are from ERA5 and average wind speeds are from MSWX, plotted against the June-December maximum precipitation in each dataset used for trend analysis. Typhoon Odette values are highlighted in red.

https://doi.org/10.5194/egusphere-2025-6337
Preprint. Discussion started: 3 February 2026

Funding

This research was funded by Uplift. RT and NS additionally received funding from the Singapore Green Finance Center, Natual Environmental Reseach Council (Grant number: NE/W009587/1) and the Vodafone Foundation.

Author contribution

All authors were involved in study conception and reviewing the manuscript. SL carried out the analysis and prepared most figures in section 2. BC carried out the analysis and prepared all figures in section 3 and a figure in section 2, and prepared the manuscript. RT and NS carried out the analysis and prepared all figures in section 4.

https://doi.org/10.5194/egusphere-2025-6337
Preprint. Discussion started: 3 February 2026

References

Baldwin, J.W., Lee, C.-Y., Walsh, B.J., Camargo, S.J., Sobel, A.H., 2023. Vulnerability in a Tropical Cyclone Risk Model: Philippines Case Study. Weather, Climate, and Society 15, 503–523. https://doi.org/10.1175/WCAS-D-22-0049.1

Basconcillo, J., Moon, I.-J., 2021. Recent increase in the occurrences of Christmas typhoons in the Western North Pacific. Sci Rep 11, 7416. https://doi.org/10.1038/s41598-021-86814-x

Beck, H.E., Wood, E.F., Pan, M., Fisher, C.K., Miralles, D.G., Dijk, A.I.J.M. van, McVicar, T.R., Adler, R.F., 2019. MSWEP V2 Global 3-Hourly 0.1° Precipitation: Methodology and Quantitative Assessment 100. https://doi.org/10.1175/BAMS-D-17-0138.1

Ciavarella, A., Cotterill, D., Stott, P., Kew, S., Philip, S., van Oldenborgh, G.J., Skålevåg, A., Lorenz, P., Robin, Y., Otto, F., Hauser, M., Seneviratne, S.I., Lehner, F., Zolina, O., 2021. Prolonged Siberian heat of 2020 almost impossible without human influence. Climatic Change 166, 9. https://doi.org/10.1007/s10584-021-03052-w

Cinco, T.A., De Guzman, R.G., Ortiz, A.M.D., Delfino, R.J.P., Lasco, R.D., Hilario, F.D., Juanillo, E.L., Barba, R., Ares, E.D., 2016. Observed trends and impacts of tropical cyclones in the Philippines. Intl Journal of Climatology 36, 4638–4650. https://doi.org/10.1002/joc.4659

Clarke, B., Zachariah, M., Barnes, C., Sparks, N., Toumi, R., Yang, W., Vahlberg, M., Lagmay, A.M., Ybañez, R., Delmendo, P.A., al, et, 2024. Climate change increased Typhoon Gaemi's wind speeds and rainfall, with devastating impacts across the western Pacific region. https://doi.org/10.25561/114170

Delfino, R.J., Vidale, P.L., Bagtasa, G., Hodges, K., 2023. Response of damaging Philippines tropical cyclones to a warming climate using the pseudo global warming approach. Clim Dyn 61, 3499–3523. https://doi.org/10.1007/s00382-023-06742-6

Eberenz, S., Lüthi, S., Bresch, D.N., 2021. Regional tropical cyclone impact functions for globally consistent risk assessments. Natural Hazards and Earth System Sciences 21, 393–415. https://doi.org/10.5194/nhess-21-393-2021

Esteban, M., Valdez, J., Tan, N., Rica, A., Vasquez, G., Jamero, L., Valenzuela, P., Sumalinog, B., Ruiz, R., Geera, W., Chadwick, C., Spatarau, C., Shibayama, T., 2023. Field Survey of 2021 Typhoon Rai -Odette-in the Philippines. Journal of Coastal and Riverine Flood Risk 1. https://doi.org/10.48438/jcrfr.2023.0001

Faranda, D., Bourdin, S., Ginesta, M., Krouma, M., Noyelle, R., Pons, F., Yiou, P., Messori, G., 2022. A climate-change attribution retrospective of some impactful weather extremes of 2021. Weather and Climate Dynamics 3, 1311–1340. https://doi.org/10.5194/wcd-3-1311-2022

Frame, D.J., Wehner, M.F., Noy, I., Rosier, S.M., 2020. The economic costs of Hurricane Harvey attributable to climate change. Climatic Change 160, 271–281. https://doi.org/10.1007/s10584-020-02692-8

Funk, C., Peterson, P., Landsfeld, M., Pedreros, D., Verdin, J., Shukla, S., Husak, G., Rowland, J., Harrison, L., Hoell, A., Michaelsen, J., 2015. The climate hazards infrared precipitation with stations—a new environmental record for monitoring extremes. Sci Data 2, 150066. https://doi.org/10.1038/sdata.2015.66

Ginesta, M., Yiou, P., Messori, G., Faranda, D., 2023. A methodology for attributing severe extratropical cyclones to climate change based on reanalysis data: the case study of storm Alex 2020. Clim Dyn 61, 229–253. https://doi.org/10.1007/s00382-022-06565-x

Global Climate Risk Index 2020 Who Suffers Most from Extreme Weather Events? Wether-Related Loss Events in 2018 and 1999 to 2018 (Briefing paper), 2021. . Germanwatch, Bonn.

Haarsma, R.J., Roberts, M.J., Vidale, P.L., Senior, C.A., Bellucci, A., Bao, Q., Chang, P., Corti, S., Fučkar, N.S., Guemas, V., von Hardenberg, J., Hazeleger, W., Kodama, C., Koenigk, T., Leung, L.R., Lu, J., Luo, J.-J., Mao, J., Mizielinski, M.S., Mizuta, R., Nobre, P., Satoh, M., Scoccimarro, E., Semmler, T., Small, J., von Storch, J.-S., 2016. High Resolution Model Intercomparison Project (HighResMIP v1.0) for CMIP6. Geoscientific Model Development 9, 4185–4208. https://doi.org/10.5194/gmd-9-4185-2016

Hansen, J., Ruedy, R., Sato, M., Lo, K., 2010. Global Surface Temperature Change. Reviews of Geophysics 48. https://doi.org/10.1029/2010RG000345

Harrington, L.J., Otto, F.E.L., Cowan, T., Hegerl, G.C., 2019. Circulation analogues and uncertainty in the time-evolution of extreme event probabilities: evidence from the 1947 Central European heatwave. Clim Dyn 53, 2229–2247. https://doi.org/10.1007/s00382-019-04820-2

https://doi.org/10.5194/egusphere-2025-6337
Preprint. Discussion started: 3 February 2026

Healey, S., Lloyd, S., Gray, J., Opdyke, A., 2022. A census-based housing vulnerability index for typhoon hazards in the Philippines. Progress in Disaster Science 13, 100211. https://doi.org/10.1016/j.pdisas.2021.100211

Hersbach, H., Bell, B., Berrisford, P., Hirahara, S., Horányi, A., Muñoz-Sabater, J., Nicolas, J., Peubey, C., Radu, R., Schepers, D., Simmons, A., Soci, C., Abdalla, S., Abellan, X., Balsamo, G., Bechtold, P., Biavati, G., Bidlot, J., Bonavita, M., De Chiara, G., Dahlgren, P., Dee, D., Diamantakis, M., Dragani, R., Flemming, J., Forbes, R., Fuentes, M., Geer, A., Haimberger, L., Healy, S., Hogan, R.J., Hólm, E., Janisková, M., Keeley, S., Laloyaux, P., Lopez, P., Lupu, C., Radnoti, G., de Rosnay, P., Rozum, I., Vamborg, F., Villaume, S., Thépaut, J.-N., 2020. The ERA5 global reanalysis. Quarterly Journal of the Royal Meteorological Society 146, 1999–2049. https://doi.org/10.1002/qj.3803

Kawase, H., Yamaguchi, M., Imada, Y., Hayashi, S., Murata, A., Nakaegawa, T., Miyasaka, T., Takayabu, I., 2021. Enhancement of Extremely Heavy Precipitation Induced by Typhoon Hagibis (2019) due to Historical Warming. SOLA - Scientific Online Letters on the Atmosphere 17A, 7–13. https://doi.org/10.2151/sola.17A-002

Kharin, V.V., Flato, G.M., Zhang, X., Gillett, N.P., Zwiers, F., Anderson, K.J., 2018. Risks from Climate Extremes Change Differently from 1.5°C to 2.0°C Depending on Rarity. Earth's Future 6, 704–715. https://doi.org/10.1002/2018EF000813

Kim, G., Cha, D.-H., Park, C., Jin, C.-S., Lee, D.-K., Suh, M.-S., Oh, S.-G., Hong, S.-Y., Ahn, J.-B., Min, S.-K., Kang, H.-S., 2021. Evaluation and Projection of Regional Climate over East Asia in CORDEX-East Asia Phase I Experiment. Asia-Pacific J Atmos Sci 57, 119–134. https://doi.org/10.1007/s13143-020-00180-8

Kossin, J.P., Emanuel, K.A., Camargo, S.J., 2016. Past and Projected Changes in Western North Pacific Tropical Cyclone Exposure. Journal of Climate 29, 5725–5739. https://doi.org/10.1175/JCLI-D-16-0076.1

Lagmay, A.M.F., Agaton, R.P., Bahala, M.A.C., Briones, J.B.L.T., Cabacaba, K.M.C., Caro, C.V.C., Dasallas, L.L., Gonzalo, L.A.L., Ladiero, C.N., Lapidez, J.P., Mungcal, M.T.F., Puno, J.V.R., Ramos, M.M.A.C., Santiago, J., Suarez, J.K., Tablazon, J.P., 2015. Devastating storm surges of Typhoon Haiyan. International Journal of Disaster Risk Reduction 11, 1–12. https://doi.org/10.1016/j.ijdrr.2014.10.006

Lenssen, N.J.L., Schmidt, G.A., Hansen, J.E., Menne, M.J., Persin, A., Ruedy, R., Zyss, D., 2019. Improvements in the GISTEMP Uncertainty Model. Journal of Geophysical Research: Atmospheres 124, 6307–6326. https://doi.org/10.1029/2018JD029522

Li, S., Otto, F.E.L., 2022. The role of human-induced climate change in heavy rainfall events such as the one associated with Typhoon Hagibis. Climatic Change 172, 7. https://doi.org/10.1007/s10584-022-03344-9

Luu, L.N., Scussolini, P., Kew, S., Philip, S., Hariadi, M.H., Vautard, R., Van Mai, K., Van Vu, T., Truong, K.B., Otto, F., van der Schrier, G., van Aalst, M.K., van Oldenborgh, G.J., 2021. Attribution of typhoon-induced torrential precipitation in Central Vietnam, October 2020. Climatic Change 169, 24. https://doi.org/10.1007/s10584-021-03261-3

Markus, Z., Rauthe-Schöch, A., Hänsel, S., Finger, P., Rustemeier, E., Schneider, U., 2022. GPCC Full Data Daily Version 2022 at 1.0°: Daily Land-Surface Precipitation from Rain-Gauges built on GTS-based and Historic Data: Globally Gridded Daily Totals. https://doi.org/10.5676/DWD_GPCC/FD_D_V2022_100

Nakamura, R., Shibayama, T., Esteban, M., Iwamoto, T., 2016. Future typhoon and storm surges under different global warming scenarios: case study of typhoon Haiyan (2013). Nat Hazards 82, 1645–1681. https://doi.org/10.1007/s11069-016-2259-3

O'Gorman, P.A., Schneider, T., 2009. Scaling of Precipitation Extremes over a Wide Range of Climates Simulated with an Idealized GCM. Journal of Climate 22, 5676–5685. https://doi.org/10.1175/2009JCLI2701.1

Otto, F.E.L., Barnes, C., Philip, S., Kew, S., van Oldenborgh, G.J., Vautard, R., 2024. Formally combining different lines of evidence in extreme-event attribution. Advances in Statistical Climatology, Meteorology and Oceanography 10, 159–171. https://doi.org/10.5194/ascmo-10-159-2024

Perkins-Kirkpatrick, S.E., Stone, D.A., Mitchell, D.M., Rosier, S., King, A.D., Lo, Y.T.E., Pastor-Paz, J., Frame, D., Wehner, M., 2022. On the attribution of the impacts of extreme weather events to anthropogenic climate change. Environ. Res. Lett. 17, 024009. https://doi.org/10.1088/1748-9326/ac44c8

Philip, S., Kew, S., van Oldenborgh, G.J., Otto, F., Vautard, R., van der Wiel, K., King, A., Lott, F., Arrighi, J., Singh, R., van Aalst, M., 2020. A protocol for probabilistic extreme event attribution analyses. Advances in Statistical Climatology, Meteorology and Oceanography 6, 177–203. https://doi.org/10.5194/ascmo-6-177-2020

https://doi.org/10.5194/egusphere-2025-6337
Preprint. Discussion started: 3 February 2026

Philippines - Typhoon Yolanda/Haiyan Fact Sheet #8, Fiscal Year (FY) 2014 - Philippines | ReliefWeb [WWW Document], 2013. URL https://reliefweb.int/report/philippines/philippines-typhoon-yolandahaiyan-fact-sheet-8-fiscal-year-fy-2014 (accessed 11.11.25).

Philippines: Super Typhoon Rai (Odette) - Situation Report No. 8 (As of 27 April 2022) - Philippines | ReliefWeb [WWW Document], 2022. URL https://reliefweb.int/report/philippines/philippines-super-typhoon-rai-odette-situation-report-no-8-27-april-2022 (accessed 11.11.25).

Philippines: Typhoon Rai (Odette) - Emergency Appeal No. MDRPH045 - Final Report - Philippines | ReliefWeb [WWW Document], 2024. URL https://reliefweb.int/report/philippines/philippines-typhoon-rai-odette-emergency-appeal-no-mdrph045-final-report (accessed 11.11.25).

Santos, C.T., Toda, L., Orduña, J.R., Santos, F.D., Ferrão, J., 2015. The impacts of Typhoon Haiyan in the Philippines: Implications to land use planning. CDDJ 1, 57–66. https://doi.org/10.18783/cddj.v001.i01.a06

Santos, G.D.C., 2025. Typhoon Odette (Rai): Rapid Intensification, Devastation, and Lessons for Resilient Recovery in the Philippines. Tropical Cyclone Research and Review. https://doi.org/10.1016/j.tcrr.2025.11.003

Santos, G.D.C., 2021. 2020 tropical cyclones in the Philippines: A review. Tropical Cyclone Research and Review 10, 191–199. https://doi.org/10.1016/j.tcrr.2021.09.003

Seriño, M.N.V., Cavero, J.A., Cuizon, J., Ratilla, T.C., Ramoneda, B.M., Bellezas, M.H.I., Ceniza, M.J.C., 2021. Impact of the 2013 super typhoon haiyan on the livelihood of small-scale coconut farmers in Leyte island, Philippines. International Journal of Disaster Risk Reduction 52, 101939. https://doi.org/10.1016/j.ijdrr.2020.101939

Shepherd, T.G., 2019. Storyline approach to the construction of regional climate change information. Proceedings of the Royal Society A: Mathematical, Physical and Engineering Sciences 475, 20190013. https://doi.org/10.1098/rspa.2019.0013

Shepherd, T.G., 2016. A Common Framework for Approaches to Extreme Event Attribution. Curr Clim Change Rep 2, 28–38. https://doi.org/10.1007/s40641-016-0033-y

Sparks, N., Toumi, R., 2025. Climate change attribution of Typhoon Haiyan with the Imperial College Storm Model. Atmospheric Science Letters 26, e1285. https://doi.org/10.1002/asl.1285

Sparks, N., Toumi, R., 2024. The Imperial College Storm Model (IRIS) Dataset. Sci Data 11, 424. https://doi.org/10.1038/s41597-024-03250-y

Takayabu, I., Hibino, K., Sasaki, H., Shiogama, H., Mori, N., Shibutani, Y., Takemi, T., 2015. Climate change effects on the worst-case storm surge: a case study of Typhoon Haiyan. Environ. Res. Lett. 10, 064011. https://doi.org/10.1088/1748-9326/10/6/064011

Tangang, F., Chung, J.X., Juneng, L., Supari, Salimun, E., Ngai, S.T., Jamaluddin, A.F., Mohd, M.S.F., Cruz, F., Narisma, G., Santisirisomboon, J., Ngo-Duc, T., Van Tan, P., Singhruck, P., Gunawan, D., Aldrian, E., Sopaheluwakan, A., Grigory, N., Remedio, A.R.C., Sein, D.V., Hein-Griggs, D., McGregor, J.L., Yang, H., Sasaki, H., Kumar, P., 2020. Projected future changes in rainfall in Southeast Asia based on CORDEX–SEA multi-model simulations. Clim Dyn 55, 1247–1267. https://doi.org/10.1007/s00382-020-05322-2

Trenberth, K.E., Dai, A., Rasmussen, R.M., Parsons, D.B., 2003. The Changing Character of Precipitation. https://doi.org/10.1175/BAMS-84-9-1205

van Oldenborgh, G.J., van der Wiel, K., Kew, S., Philip, S., Otto, F., Vautard, R., King, A., Lott, F., Arrighi, J., Singh, R., van Aalst, M., 2021. Pathways and pitfalls in extreme event attribution. Climatic Change 166, 13. https://doi.org/10.1007/s10584-021-03071-7

Vautard, R., Yiou, P., Otto, F., Stott, P., Christidis, N., van Oldenborgh, G.J., Schaller, N., 2016. Attribution of human-induced dynamical and thermodynamical contributions in extreme weather events. Environ. Res. Lett. 11, 114009. https://doi.org/10.1088/1748-9326/11/11/114009

Wang, C.-C., Tseng, L.-S., Huang, C.-C., Lo, S.-H., Chen, C.-T., Chuang, P.-Y., Su, N.-C., Tsuboki, K., 2019. How much of Typhoon Morakot's extreme rainfall is attributable to anthropogenic climate change? International Journal of Climatology 39, 3454–3464. https://doi.org/10.1002/joc.6030

Wehner, M.F., Zarzycki, C., Patricola, C., 2019. Estimating the Human Influence on Tropical Cyclone Intensity as the Climate Changes, in: Collins, J.M., Walsh, K. (Eds.), Hurricane Risk. Springer International Publishing, Cham, pp. 235–260. https://doi.org/10.1007/978-3-030-02402-4_12

https://doi.org/10.5194/egusphere-2025-6337
Preprint. Discussion started: 3 February 2026

Yamaguchi, M., Maeda, S., 2020. Slowdown of Typhoon Translation Speeds in Mid-latitudes in September Influenced by the Pacific Decadal Oscillation and Global Warming. Journal of the Meteorological Society of Japan 98, 1321–1334. https://doi.org/10.2151/jmsj.2020-068

Yi, C.J., Suppasri, A., Kure, S., Bricker, J.D., Mas, E., Quimpo, M., Yasuda, M., 2015. Storm surge mapping of typhoon Haiyan and its impact in Tanauan, Leyte, Philippines. International Journal of Disaster Risk Reduction 13, 207–214. https://doi.org/10.1016/j.ijdrr.2015.05.007

Yiou, P., Jézéquel, A., Naveau, P., Otto, F.E.L., Vautard, R., Vrac, M., 2017. A statistical framework for conditional extreme event attribution. Advances in Statistical Climatology, Meteorology and Oceanography 3, 17–31. https://doi.org/10.5194/ascmo-3-17-2017

Zhang, W., Vecchi, G.A., Murakami, H., Delworth, T.L., Paffendorf, K., Jia, L., Villarini, G., Gudgel, R., Zeng, F., Yang, X., 2016. Influences of Natural Variability and Anthropogenic Forcing on the Extreme 2015 Accumulated Cyclone Energy in the Western North Pacific. Bulletin of the American Meteorological Society 97, S131–S135. https://doi.org/10.1175/BAMS-D-16-0146.1

Zscheischler, J., Lehner, F., 2022. Attributing Compound Events to Anthropogenic Climate Change. Bulletin of the American Meteorological Society 103, E936–E953. https://doi.org/10.1175/BAMS-D-21-0116.1